Journal of Molecular Catalysis A: Chemical 324 (2010) 104–119

Contents lists available at ScienceDirect

Journal of Molecular Catalysis A: Chemical

journal homepage: www.elsevier.com/locate/molcata

Computational catalysis

Real size of ligands, reactants and catalysts: Studies of structure, reactivity and selectivity by ONIOM and other hybrid computational approaches☆

Valentine P. Ananikov[a], Djamaladdin G. Musaev[b], Keiji Morokuma[b,*]

[a] N.D. Zelinsky Institute of Organic Chemistry, Russian Academy of Sciences, Leninsky Prospect 47, Moscow 119991, Russia
[b] Cherry L. Emerson Center for Scientific Computation and Department of Chemistry, Emory University, Atlanta, GA 30322, USA

ARTICLE INFO

Article history:
Available online 15 March 2010

Keywords:
Catalysis
ONIOM
Transition metal complexes
Nanoparticles
Zeolites

ABSTRACT

Application of hybrid ONIOM, QM/QM and QM/MM theoretical methods to study catalytic reactions involving molecular, nano-sized and supported transition metal catalysts are reviewed. The best strategies for theoretical studies of full size chemical systems (without simplifying structural approximations and avoiding the usage of unreliable small size models) are highlighted. The influence of the steric and electronic effects of ligands, reactants and molecular environment on reactivity of transition metal catalysts is discussed.

© 2010 Elsevier B.V. All rights reserved.

Contents

1. Introduction

The progress in catalysis and transition metal chemistry is hardly possible without understanding of the mechanisms of chemical transformations at molecular level. Accurate information about structure, properties, reactivity and relative energies of the species involved in the reaction – initial complexes, intermediates and products – is a requirement for any mechanistic study and for design of more efficient catalytic processes. Currently, structure and properties of stable complexes are a subject of routine measurements with modern analytic tools. However, lack of reliable experimental techniques to obtain an accurate knowledge on transient species as well as specific transition states is one of bottlenecks of real progress in the designing of better and more efficient catalysts.

Development of theoretical methods and rapid increase of computational power in recent decades made it possible to carry out

Abbreviations: 6-31+G(d,p), etc., polarized split-valence basis sets according to Pople; acac, acetylacetonate; B3LYP, etc., density functionals; bpy, 2,2′-bipyridyl ligand; CASSCF, complete active apace multiconfiguration self-consistent field; CCSD(T), coupled cluster calculations using single and double substitutions and triple excitations; CEP-31G, Stevens/Basch/Krauss effective core potential; D95, Dunning/Huzinaga double zeta bases set; DFT, density functional theory; dz+p, double-ζ plus polarization basis set; EXSY, two-dimensional NMR exchange spectroscopy; GIAO, gauge-including atomic orbitals; HF, Hartree–Fock; QM, quantum mechanics; Lanl2mb, Los Alamos effective core potential plus minimal bases set; Lanl2dz, Los Alamos effective core potential plus double-ζ bases set; MD, molecular dynamics; MM, molecular mechanics; MOF, metal-organic frameworks; MP2, second-order Møller–Plesset correlation energy correction; MP4(SDQ), fourth-order Møller–Plesset correlation energy correction for single, double and quadruple substitutions; NHC, N-heterocyclic carbene ligand; PCM, polarizable continuum model; SDD, Stuttgart/Dresden effective core potential bases set; Tp′, substituted tris(pyrazolyl)borate ligand; tz+p, triple-ζ plus polarization basis set; UFF, universal force field (molecular mechanics).

☆ This paper is part of a special issue on Computational Catalysis.

* Corresponding author. Tel.: +1 404 727 2180; fax: +1 404 727 6586.
E-mail address: morokuma@emory.edu (K. Morokuma).

1381-1169/$ – see front matter © 2010 Elsevier B.V. All rights reserved.
doi:10.1016/j.molcata.2010.03.015

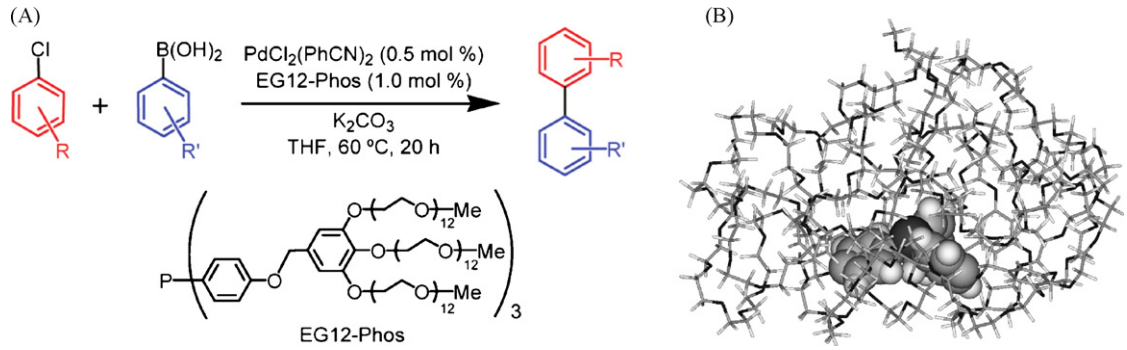

Scheme 1. (A) Catalytic Suzuki–Miyaura coupling reaction (isolated yields 89–97%); (B) ONIOM (B3LYP/Lanl2dz:UFF) optimized structure of the EG-12-Phos ligand with the triphenylphosphine core highlighted by space-filling representation [24].
© 2009 American Chemical Society. Reproduced with permission.

computational studies of these species with accuracy similar to those of experimental measurements. Currently, theoretical studies of small molecules became a powerful tool, which is very often utilized to guide complicated experimental investigations and predict new chemical reactions. However, in spite of great progress in theoretical studies of small chemical systems, studies on real-size molecular systems involved in catalysis still remain problematic. Due to technical limitations the real-size molecules still cannot be a subject of highly accurate quantum chemical investigations.

Latest development of hybrid theoretical approaches provides a real opportunity to study large molecular systems by dividing them into several subsystems (layers) and treating them at different levels of well-developed conventional computational methods. In these hybrid approaches, the most important and relatively small part of the real system, where the bond formation and bond breakage occur (the active part of the catalyst and reactants), is treated at the most accurate computational levels (high layer, i.e. quantum mechanically (QM)). Other parts (subsystems) of the real system, which are not directly involved in the studied chemical reactions, are treated at the less demanding computational levels (such as low level quantum mechanical (QM) or molecular mechanics (MM) methods). In literature, the targeted systems are often partitioned into two (high and low) or three (high, medium and low) subsystems, and the resulted hybrid methods called (in two-layer approach) as QM/QM, QM/MM, ONIOM(QM:QM) or ONIOM (QM:MM). As pointed out in many theoretical papers, utilization of the well-developed hybrid approaches significantly speeds up the calculations and overcomes the size-limitation in computational studies [1,2].

Several implementations of the hybrid QM/QM and QM/MM approaches are available [3–6] and their applications to study metal-containing systems have been widely reviewed [7–11]. A more specialized reviews on the application of hybrid methods in inorganic chemistry [12], in substitution and rearrangement reactions [13], in selectivity of organic and bioorganic reactions [14], in modeling of zeolites [15], in computation of transition metal NMR chemical shifts [16], and in studies of biological systems [17–20] are also available. A compilation of available software to carry out hybrid calculations has been also published [21].

The subject of our review is the application of the hybrid methods to reveal the role of molecular environment in ligands, reactants and metal complexes. We discuss what properties of transition metal complexes can be calculated, which theory levels should be utilized and what accuracy can be expected. The discussion is based on recent studies published in 2008–2009 and utilizing ONIOM as well as other hybrid approaches.

2. Hybrid theoretical methods in the studies of transition metal systems

The first two sections of this review highlight the influence of ligand structure (Section 2.1), and reactants (Section 2.2) on catalytic activity of transition metal systems. The next sections describe a more complicated multinuclear metal species (Section 2.3) and reactions on surfaces (Section 2.4). In the final sections we summarize the information on the theory levels used, and recent developments in the hybrid methodology (Sections 2.5 and 2.6, respectively).

2.1. The influence of ligand structure on catalytic activity of transition metal systems

Ligands of transition metal centers can strongly influence reactivity of transition metal complexes by altering electronic structure of the transition metal atoms, by preventing the coordination sphere of the metal centers from full saturation, and/or by directly involving into catalytic process as an alternative reactive center. Here we discuss the role of the size and type of widely used ligands in catalysis.

The size of ligands could be crucial in stabilization of coordinatively unsaturated transition metal complexes, which are known to show enhanced catalytic activities compared with their coordinatively saturated analogs. Typical ways to generate such reactive species are: (a) to add the required amount of ligand to the ligand-free metal precursor, for example usage of Pd_2dba_3:PR_3 = 1:4 mixture to generate $Pd(PR_3)_2$ (see, for example Refs. [22,23]), or (b) to design a specific ligand (with a massive shape and large steric bulkiness), coordination of which to the transition metal center prevents coordination of other ligands to the metal while allowing the binding of the reactants [24,25]. For example, it was shown that the use of modified triphenyl phosphine ligand bearing dodeca(ethylene glycol) chains (EG-12-Phos ligand) significantly enhances the catalyst efficiency in Suzuki–Miyaura coupling reaction (Scheme 1) [24]. Connolly solvent-excluded volumes of the pure PPh_3 and EG-12-Phos ligands were calculated to be 230 and 6720 Å^3, respectively [24]. ONIOM(B3LYP/Lanl2dz:UFF) calculations revealed the structure of this ligand: it was found that folded structure of the ligand was by 68 kcal mol^{-1} more stable than its linear chains structure (Scheme 1). These calculations confirmed a gigantic size of the modified ligand compared to a small phosphine ligands usually used in the Suzuki–Miyaura coupling (and many other) reaction. The catalytic system with the EG-12-Phos ligand was found to be highly efficient for unactivated aryl chlorides as the reactant and resulted in high product yields [24]. The observed

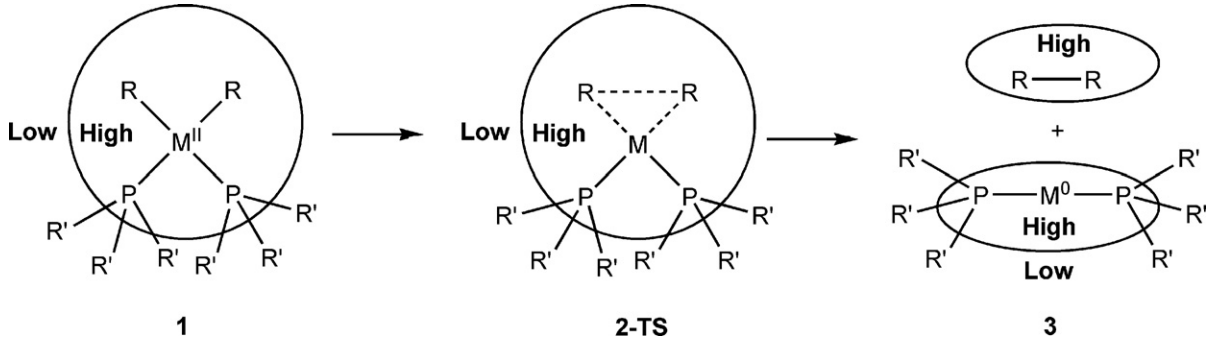

Scheme 2. High and low levels of the ONIOM calculations of C–C coupling reaction, where R′=H, Me, Ph and Cy (similar partitioning was also utilized for **4** and **5-TS** showed in Scheme 3) [29].
© 2007 Wiley-VCH Verlag GmbH & Co. KGaA. Reproduced with permission.

high catalytic activity of this system, most likely, is originated by the higher concentration of unsaturated species. A similar effect was also discussed for the tetraethylene glycol moieties attached to the phosphine [26] and NHC [27] ligands. Although it is quite useful to model linear and chain structures of the ligand and to compare their relative energies, it should be pointed out that molecular dynamics simulations would provide more accurate description of the system.

Computational study of C–C bond activation by $[RuL_2(PPh_3)(CO)(H)_2]$ complex provided an impressive illustration of the ligand effect on formation of unsaturated species and altering the reactivity of the metal complex [28]. Comparing calculations of small model system with full size system at ONIOM level it was reported that each PPh_3/NHC substitution in the ligand L labilizes the remaining Ru–PPh_3 bond by about 10 kcal mol^{-1} (NHC = 1,3-dimesitylimidazol-2-ylidene; IMes). The easier PPh_3 ligand loss was attributed to the increased steric repulsions in the complex. Mechanistic study showed that the presence of the NHC ligands did not directly promote C–C bond activation step, but rather it facilitates formation of highly reactive 14e unsaturated intermediate $[Ru(NHC)_2(CO)]$ due to PPh_3 dissociation and H_2 loss from the initial structure. This unsaturated intermediate was very reactive towards the C–C bond activation [28].

Previously, by utilizing of two-layer ONIOM approach we have shown that ligands of transition metal centers may effect not only the structure and energetic parameters of reactants, intermediates, transition states and products of the reaction, but also may completely alter the reaction pathway (Scheme 2) [29]. In this study, geometries of the proposed reactants, intermediates, transition states and products of the C–C coupling reaction in $[Pd(CH_3)_2(PR_3)_2]$ were optimized at the ONIOM(B3LYP:HF) level. Their energetics was calculated at the ONIOM(B3LYP:B3LYP) level, with different basis sets for the model and real systems, at the ONIOM(B3LYP:HF) optimized geometries. It was found that Pd–P binding energy was of much importance for the reaction mechanism.

As seen in Scheme 3, in general, the C–C coupling in these complexes may proceed via two distinct pathways involving coordinatively saturated (four-coordinated: **1** → **2-TS** → **3**) and coordinatively unsaturated (three-coordinated: **1** → **4** → **5-TS** → **3**) intermediates. The calculations shown that energy barrier associated with the C–C reductive elimination follows the trend for the four-coordinative pathway: L = PPh_3 ($\Delta H^{\neq}$ = 22.2 kcal mol^{-1}) < L = PH_3 ($\Delta H^{\neq}$ = 24.2 kcal mol^{-1}) < L = PCy_3 ($\Delta H^{\neq}$ = 27.4 kcal mol^{-1}) < L = PMe_3 ($\Delta H^{\neq}$ = 29.1 kcal mol^{-1}). However, in the case of the three-coordinated pathway the complex with tricyclohexylphosphine ligand becomes more reactive and energy barrier associated with the C–C reductive elimination changes in the following trend: L = PCy_3 ($\Delta H^{\neq}$ = 21.9 kcal mol^{-1}) < L = PPh_3 ($\Delta H^{\neq}$ = 24.2 kcal mol^{-1}) < L = PH_3 ($\Delta H^{\neq}$ = 26.9 kcal mol^{-1}) < L = PMe_3 ($\Delta H^{\neq}$ = 30.8 kcal mol^{-1}) [30]. Which of these pathways is going to be operative was determined by the strength of the Pd–PR_3 bond; dissociation enthalpy of the Pd–PR_3 bond in complex $[Pd(CH_3)_2(PR_3)_2]$ decreases in the order: L = PMe_3 (ΔH = 18.8 kcal mol^{-1}) > L = PH_3 (ΔH = 15.0 kcal mol^{-1}) > L = PPh_3 (ΔH = 12.1 kcal mol^{-1}) > L = PCy_3 (ΔH = 10.6 kcal mol^{-1}). From these calculated results it is clear that C–C coupling in $[Pd(CH_3)_2(PCy_3)_2]$ prefers the three-coordinated pathway because of relatively smaller PCy_3 dissociation energy (compared with other studied phosphine ligands).

It should be pointed out that generation of unsaturated Ru species with NHC ligands was utilized in C–C bond breakage reaction (see Ref. [28] and the discussion above), while formation of unsaturated species in Pd/phosphine system facilitated C–C bond-formation reaction [29]. In both cases the reactivity of the metal complexes was enhanced through ligand dissociation and formation of unsaturated species. Clearly, the further computational mechanistic studies are required to reveal a general concept of the reactivity of unsaturated transition metal complexes and understand the role of metal/ligand effect.

Comparative structural study of the hydride complexes of Ru has shown that even subtle changes in the size of ligand may trigger the mode of coordination (Scheme 4) [31]. For L = PPh_2, the most stable isomer of the complex $(H)_2Ru(PR'_3)_2(LCH_2BHR)$ was the $\mathbf{A_L}$ form, while its $\mathbf{B_L}$ and $\mathbf{C_L}$ isomers were calculated to be higher in energy by 7.5 and 1.9 kcal mol^{-1}, respectively. Surprisingly, for L = SMe a coupling of the *cis*-hydride and borohydride ligands was observed and an analog of the isomer $\mathbf{B_L}$ with two B-H bonds became the most

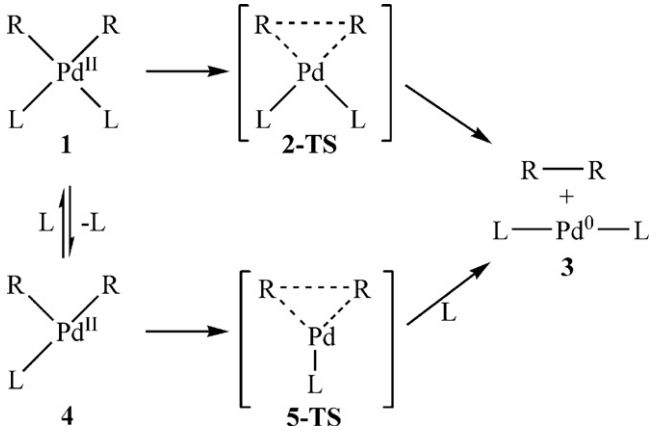

Scheme 3. Carbon–carbon bond formation through the four-coordinate and three-coordinate pathways (L = PH_3, PMe_3, PPh_3 and PCy_3) [29].
© 2007 Wiley-VCH Verlag GmbH & Co. KGaA. Reproduced with permission.

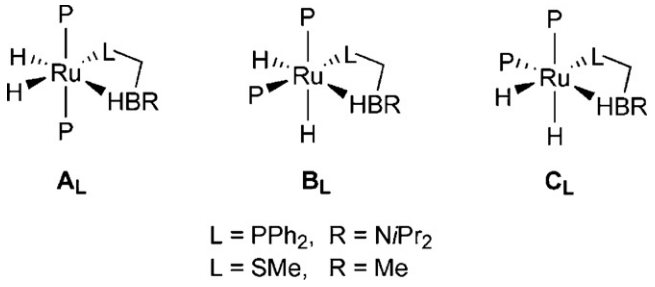

Scheme 4. Different isomers of the Ru complex due to ligand interactions [31].
© 2009 Wiley-VCH Verlag GmbH & Co. KGaA. Reproduced with permission.

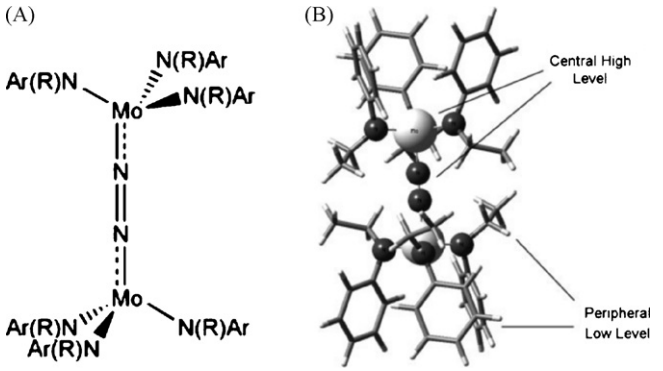

Fig. 1. (A) The structure of the μ-N_2 intermediate in nitrogen activation mechanism; (B) ONIOM partitioning of the complex (Ar=Ph, R=Et) [36].
© 2009 Wiley Periodicals, Inc. Reproduced with permission.

stable compound, while the isomers $\mathbf{A_L}$ and $\mathbf{C_L}$ were calculated to be higher in energy by 12.0 and 4.1 kcal mol^{-1}, respectively [31]. The results of this theoretical study were in excellent agreement with the experimental X-ray analysis, thus, confirming the reliable choice of the ONIOM calculations for revealing structural effects in these metal complexes.

Ligand exchange reactions may also have pronounced effect on the reactivity of transition metal complexes. Understanding the nature of the concurrent binding of the phosphine ligand and CO is of much importance to rationalize the mechanism of carbonylation. It was reported that the mechanism of this reaction may involve rate-determining PPh_3 dissociation from the $[Co_2(CO)_5(CH–COOEt)(PPh_3)_2]$ complex followed by fast coordination of CO [32]. At the ONIOM level, the dissociation of the triphenylphosphine ligand was found to proceed barrierless with $\Delta G = 5.9$ kcal mol^{-1}. The ONIOM study has also addressed the mechanism of CO ligands exchange involving both terminal and bridging ligands [32]. Depending on the type of cobalt complex and ligands rather different values of free energy of CO dissociation were calculated: 7.5, 14.9, 19.7, and 30.1 kcal mol^{-1} [33].

Dynamical environmental effects of the ligands were studied with ONIOM-MD calculations. Molecular dynamics calculations at the ONIOM(HF:MM3) level were carried out to study reductive elimination reaction [34] *cis*-$(H)_2Pt(PR_3)_2 \rightarrow H_2 + Pt(PR_3)_2$ and dynamic behavior of H_2 molecule in the $[PtH(H_2)(PR_3)]^+$ complex (R = H, Me, Ph, *t*Bu) [35]. In the reductive elimination reaction dynamic effects increased the reactivity in the order: *t*Bu > Ph > Me > H [34]. In the second case, the dynamic environmental effect of the large P(*t*Bu)$_3$ ligand increased the energy fluctuations, thus, prompting rotation and dissociation of the coordinated H_2 molecule [35]. Interestingly, the large steric bulkiness of the ligand show its effect on the reactivity in such pronounced way, which is usually neglected in typical calculations of the static structures.

Different electronic structure methods can be combined within the ONIOM approach. This feature is especially important for high accuracy levels like CCSD(T), which impose scaling restrictions for large molecular systems. Single point ONIOM[CCSD(T):B3LYP] calculations were carried on the ONIOM(B3LYP:HF) optimized geometry to gain an insight into nitrogen activation by molybdenum complexes (Fig. 1) [36].

The potential energy surface for the nitrogen activation was in a good agreement with earlier model calculations on the molybdenum systems [37–40] and revealed important information about the ligand environment effect. The ONIOM[CCSD(T):B3LYP] calculated potential energy surface (Fig. 2) of nitrogen activation reaction by $[Mo(NRPh)_3]$ (Fig. 1) provides an excellent example of the magnitude of ligand environment effect on reaction mechanism and clearly confirms the benefits of the hybrid method to understand ligand effect. Interesting to point out, the study has shown that ligand environment acts not only in terms of steric bulk of the substituents R, but also exhibits significant electronic destabilization as the size of the ligands increases [36]. The effect of ligand environment was also evaluated in the reaction of H_2 with zirconium dinitrogen complex and compared with theoretical studies involving smaller system [41,42].

Variation of the ligand bulk can be used to suppress the reaction pathway as was demonstrated in the combined experimental and theoretical ONIOM(MP2:HF) study (Fig. 3) [43]. Introducing two *t*Bu ligands hindered the metal atom (Zn or Li) and increased the activation energy for the reaction with Br, $\Delta E^{\neq} = 29.2$ kcal mol^{-1}. With smaller size Me ligands (instead of *t*Bu ligands) the activation energy was decreased to $\Delta E^{\neq} = 23.5$ kcal mol^{-1}. Calculated reaction energy was very similar for both cases, $\Delta E = -5.0$ and -5.3 kcal mol^{-1}, respectively. Realization of the kinetic control was confirmed by experimental findings, which have shown that *t*Bu ligand inhibits the reaction [43].

Desired tuning of catalytic activity of the metal complexes can be carried by variations in the ligand structure. In Ni-catalyzed amination of C–H bond the ONIOM(B3LYP:UFF) calculations were applied to identify a suitable ligand to make the reaction thermodynamically feasible. In fact, this requires increasing the metal–amine bond strength and diminishing metal–amide bond strength [44]. Based on the results of the theoretical study promising catalyst candidates for the amination of C–H bond were predicted.

Comparison of the B3LYP calculations for the model $[\{Ti(\eta^5\text{-}C_5H_5)(\mu\text{-}O)\}_3(\mu_3\text{-}CMe)]$ complex and ONIOM(B3LYP:UFF) calculations for the real $[\{Ti(\eta^5\text{-}C_5Me_5)(\mu\text{-}O)\}_3(\mu_3\text{-}CMe)]$ system has shown that steric effect reduces rotational barrier of the alkylidene ligand from 30.9 to 24.4 kcal mol^{-1} and relative destabilization of an intermediate rises from 0.7 to 5.3 kcal mol^{-1} [45]. The origin of slipped-sandwich structure of the silyl-substituted zinconocenes $[Zn(\eta^5\text{-}Cp)(\eta^1\text{-}CpH_4R)]$ (R = SiH_xMe_{3-x}, SiH_2*t*Bu, and $SiMe_2$*t*Bu) was addressed in the DFT:MM study, where the substituents on the silicon atom were placed into the MM layer [46]. In such a case only steric effect of the substituents was taken into account in the calculation and the electronic effect was excluded. The calculations have shown that the changes in the zinconocene structure cannot originate from the steric effect, but from the electronic effect instead [46].

ONIOM methodology provides not only a convenient way to speed up the calculations, but also an excellent opportunity to distinguish steric and electronic factors of ligands on structure and reactivity of metal complexes. Typical procedure to estimate steric effect in the system of interest is to compare QM calculations on the model system with QM:MM calculations on the real system. For example, for the system with phosphine ligands it would be PH_3 and PR'_3, respectively (Scheme 5).

Two-step decomposition makes it possible to analyze both steric and electronic effects (Scheme 6). In this procedure steric effect

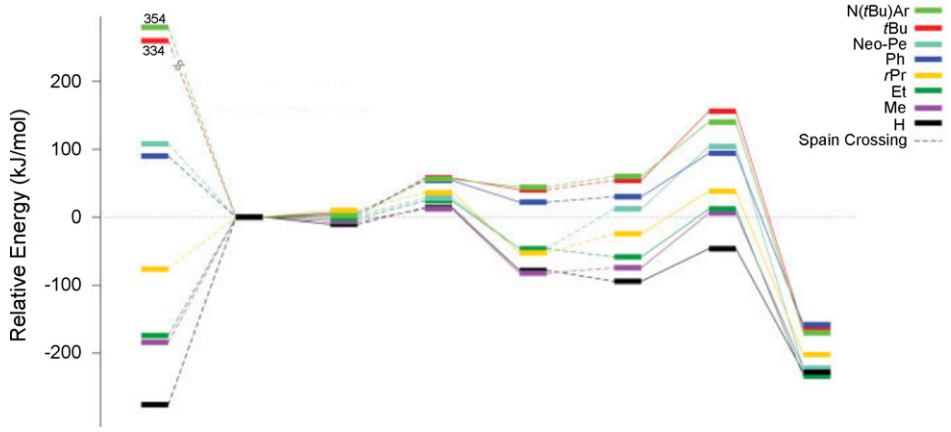

Fig. 2. Potential energy surface of the nitrogen activation reaction by [Mo(NRPh)$_3$] complex at the ONIOM(CCSD(T):B3LYP) level for different substituents [36].
© 2009 Wiley Periodicals, Inc. Reproduced with permission.

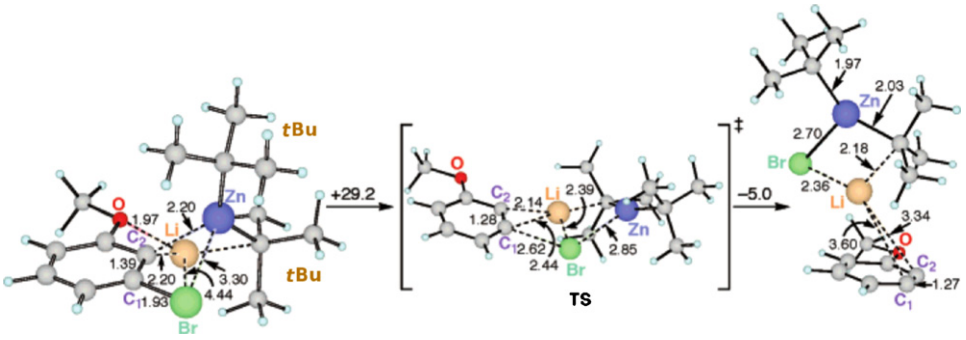

Fig. 3. Reaction path of the benzyne formation with tBu$_2$Zn(2-Br-anizole)Li: geometries optimized at the ONIOM(MP2:HF) level and single point energies at MP2 level [43].
© 2008 American Chemical Society. Reproduced with permission.

can be evaluated by comparing QM calculations for the reference point with PH_3 ligand and QM:MM calculations for the PR'_3 ligand (the same as above). The next step is to compare QM:MM decomposition point with QM:QM calculations for the real-size system—this comparison provides information about the electronic effect (Scheme 6). This approach was utilized to study C–C bond-formation involving Pd species with different steric and electronic effects of the coordinated phosphine ligands, as represented by the [Pd(Me)$_2$(PH$_3$)$_2$], [Pd(Me)$_2$(PMe$_3$)$_2$], [Pd(Me)$_2$(PPh$_3$)$_2$] and [Pd(Me)$_2$(PCy$_3$)$_2$] complexes (Fig. 4) [29]. It was found that steric effect mostly influences the initial metal complex, while electronic effect has the most impact on the transition state. Studied steric and electronic effects changed the reactivity in opposite manner: steric effect decreased the activation barriers for C–C reductive elimination, while the electronic effect increased the activation barriers [29,57].

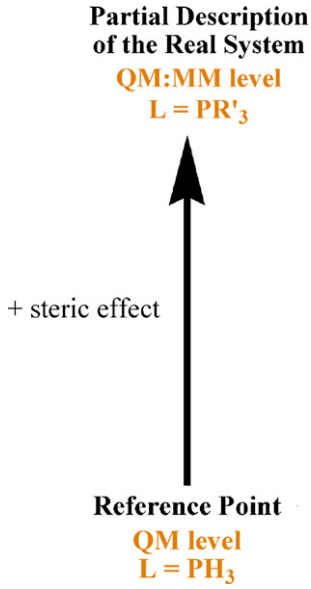

Scheme 5. Evaluation of the steric effect by hybrid QM:MM calculations (see Scheme 2 for the description of exemplified phosphine system).

Although the above description for the evaluation of steric and electronic effects was exemplified for the phosphine ligands, it is obviously suitable for the other ligands as well. Note, in order to evaluate steric and electronic effect of a particular substituent in the ligand this substituent should be placed in the low level (for example, R′ in the considered phosphine ligands; see Scheme 2) in hybrid studies.

2.2. The influence of reactant and its substituents on catalytic activity and selectivity of transition metal systems

In the previous section we have considered the role of ligands to tune the reactivity of transition metal complexes and to control the direction of the chemical transformation. Another important factor controlling reactivity of the transition metal catalysts is reactant that also influences the selectivity of the catalytic reactions.

In order to elucidate the alkenes hydrogenation/C–H bond activation mechanisms in Ir complexes the stability and geometry of Ir-NHC complexes with coordinated alkene unit were studied at the ONIOM level [47]. These calculations have revealed rather small energy difference between the coplanar and perpendicular alkene

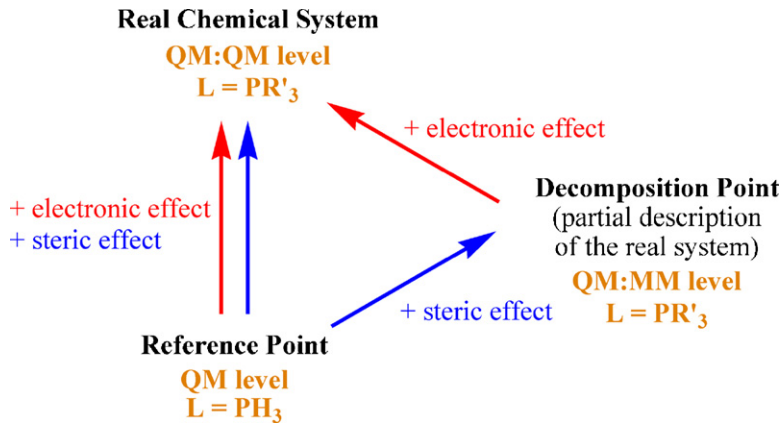

Scheme 6. Two-step decomposition to evaluate steric and electronic effect for the phosphine ligands (see Scheme 2 for the description of exemplified phosphine system).

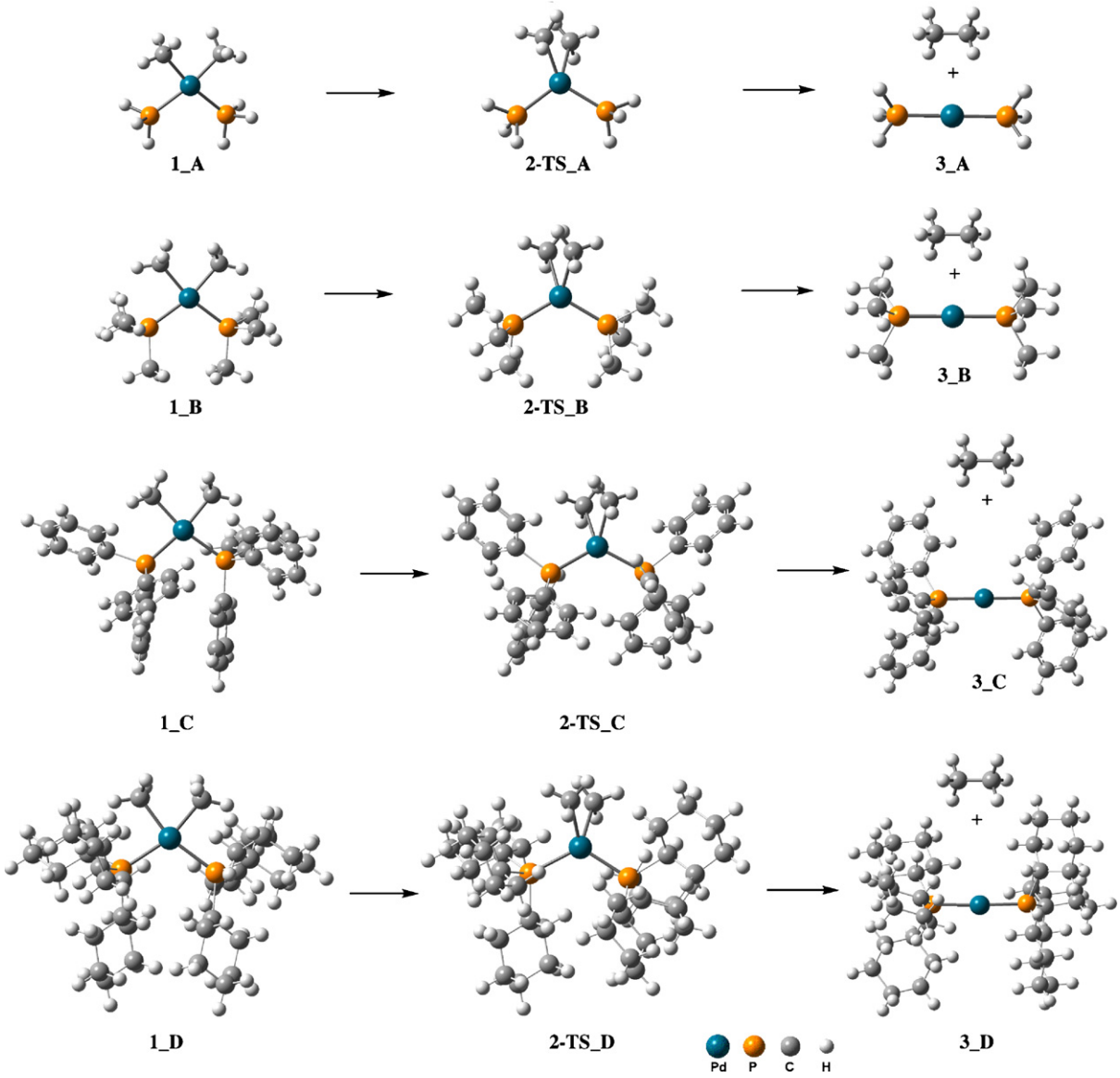

Fig. 4. ONIOM(B3LYP:HF) optimized structures of the initial complexes, transition states and products of the Me–Me coupling from the $[Pd(Me)_2L_2]$ complexes: **1_A–3_A**: $L = PH_3$; **1_B–3_B**: $L = PMe_3$; **1_C–3_C**: $L = PPh_3$; **1_D–3_D**: $L = PCy_3$ [29,57].
© 2007 Wiley-VCH Verlag GmbH & Co. KGaA. Reproduced with permission.

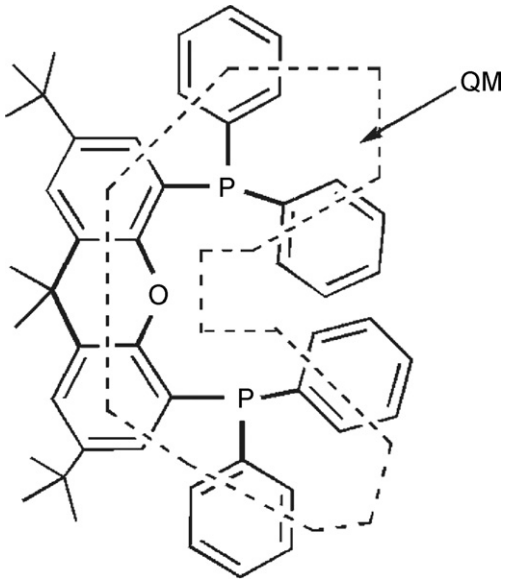

Scheme 7. ONIOM partitioning into the high (QM) and low (the rest of the molecule) levels for the xanthene ligand [49].
© 2009 American Chemical Society. Reproduced with permission.

orientations (~5 kcal mol^{-1}), and have identified the role of the steric factors in the alkene 2-position [47].

In the study of C–H bond activation by Ir/Tp′ complexes three different C–H coordination isomers of the phenyl group were characterized by ONIOM(BHandH:UFF) calculations [48]. Relative energy of the complexes resulted from *ortho*-, *meta*- and *para*-C–H bonds coordination to the metal was 0.0, 0.9 and 3.0 kcal mol^{-1}, respectively. Despite small energy difference between the studied isomers, the authors followed the pathway initiated from the *ortho*-species [48].

The key-role of the isomerization step in catalytic hydroformylation was studied with DFT and ONIOM methods [49]. As an illustration, QM:MM partitioning into the high and low levels preserving sp^2 hybridization of the carbon atoms attached to phosphorus is shown in Scheme 7. This type of partitioning was also utilized in some other studies and it should be applied to preserve correct electron donating properties of the phosphorus atom. An example of QM:MM partitioning of the porphyrin system was discussed and compared to QM calculations in the study of Mn-catalyzed alkene epoxidation [50].

It should be noted that different partitioning should be applied if separation of steric and electronic effects of the aryl groups is of interest. In such case the whole aryl group should be treated at the low level method (see Section 2.1). Therefore, careful selection of the high and low levels should be made depending on the purpose of the theoretical study. Special attention should be paid for partitioning of conjugated π-systems.

Comparison of DFT calculations on the model system and QM:MM calculations on the real system have highlighted the main features of the isomerization stage in catalytic hydroformylation reaction [49]. The xanthene ligand (Scheme 7) was found to differentiate the terminal and internal alkenes upon their coordination to Rh-centers to form η^2-Rh complexes. This ligand was found to stabilize 1-alkene species more than 2-alkene species: the calculated energy difference between these structures was ~10 kcal mol^{-1}. Higher relative concentration of η^2-(1-alkene)-Rh species was suggested as a key-factor to control the selectivity of the subsequent hydroformylation reaction. Indeed, it was reported that hydroformylation of terminal 1-alkenes proceeds more easily than hydroformylation of internal 2-alkenes [49]. The further studies on this system are anticipated, since the greater stability of the η^2-(1-alkene)-Rh species could also have an opposite effect and may hinder their reactivity.

Particularly, an interesting example of ethylene/acetylene reactant selectivity was reported for the Ir/Tp′ complexes [51]. According to the ONIOM(BHandH:UFF) calculations ethylene coordination to form the η^2-Ir complex was thermodynamically more preferred than coordination of acetylene (by ~3 kcal mol^{-1}). However, as far as the reactivity is concerned, the reaction with acetylene proceeds via the acetylene dimerization, while ethylene was not involved in the reaction and gave a stable π-complex [51].

ONIOM(B3PW91:HF) calculations on the [R–N=Ti-R′(L)]$^+$ titanium complexes have shown that, depending on the steric bulk, ethylene molecule can be oriented to react either via the cycloaddition pathway with the R–N=Ti center or via the insertion pathway involving another Ti–R′ center [52]. The cycloaddition pathway was shown to be kinetically preferred process, while the thermodynamic control can be applied by adjusting the size of substituents in the groups involved in the reaction. It is an excellent example showing that steric control can directly influence the outcome of the catalytic reaction [52].

Further studies of the mechanistic details of ethylene insertion were carried out in the zirconocene complexes [53]. Different dependence of the energy barriers on the size and positions of substituents was described for the chain transfer and chain propagation stages. The difference was shown to play an important role in producing high molecular weight polymers with ethylene/propylene homopolymerization, while low molecular weight polymers were afforded with ethylene/propylene copolymerization [53]. Molecular modeling of ethylene insertion in the generation IV/V Ziegler/Natta catalyst at the ONIOM(TPSS:UFF) level has shown that selectivity of this catalytic system may be further increased, although at a cost of activity [54]. Insertion reactions involving the double bonds of allene and vinylpyridine were studied for Ru and Os complexes with ONIOM(B3LYP:HF) calculations to estimate the difference between the model compounds with PH_3 ligands and real complexes with PPh_3 ligands [55,56].

Strong reactant influence on the C–C bond formation through the reductive elimination mechanism was reported by ONIOM(B3LYP:HF) studies [29,57,58]. The following activation energies ($\Delta H^{\neq}$) of the R–R elimination were calculated for the series of the [Pd(R)$_2$(PPh$_3$)$_2$] complexes: 3.0 kcal mol^{-1} (for R=CH=CH$_2$), 8.8 kcal mol^{-1} (for R=Ph), 12.0 kcal mol^{-1} (for R=C≡CH), and 22.2 kcal mol^{-1} (for R=Me) (Fig. 5) [29]. Clearly, a dramatic improvement in the C–C bond formation should be observed upon changing from methyl–methyl to vinyl–vinyl coupling reaction. Indeed, this finding was confirmed in a number of experimental studies in the framework of cross-coupling reactions [59]. For the Pd complexes bearing different groups R and R′ the reductive elimination from the [Pd(R)(R′)(PPh$_3$)$_2$] complexes was calculated to take place with interjacent reactivity compared to the corresponding [Pd(R)$_2$(PPh$_3$)$_2$] and [Pd(R′)$_2$(PPh$_3$)$_2$] complexes [29,57,58].

Oxidative addition of phenyl thiocyanates to Pd(PR$_3$)$_2$ complex may proceed either with breakage of Ph–SCN or PhS–CN bonds [60]. The comparison of model system with PH_3 ligand and real system with PPh_3 ligand has shown that oxidative addition of the PhS–CN bond becomes more favorable by 5.6 kcal mol^{-1} in the latter case [60]. A comparative B3LYP and ONIOM(B3LYP:HF) study was carried out for oxidative addition of carbon-halogen bonds to Pd(PR$_3$)$_2$ complex [61] and C–C coupling in the low coordination [Pd(PR$_3$)(R^1)(R^2)] complexes [62].

Reaction of organic azides R–N$_3$ with Zr [63] and Ni [64] complexes was studied at the ONIOM level. The main attention was paid

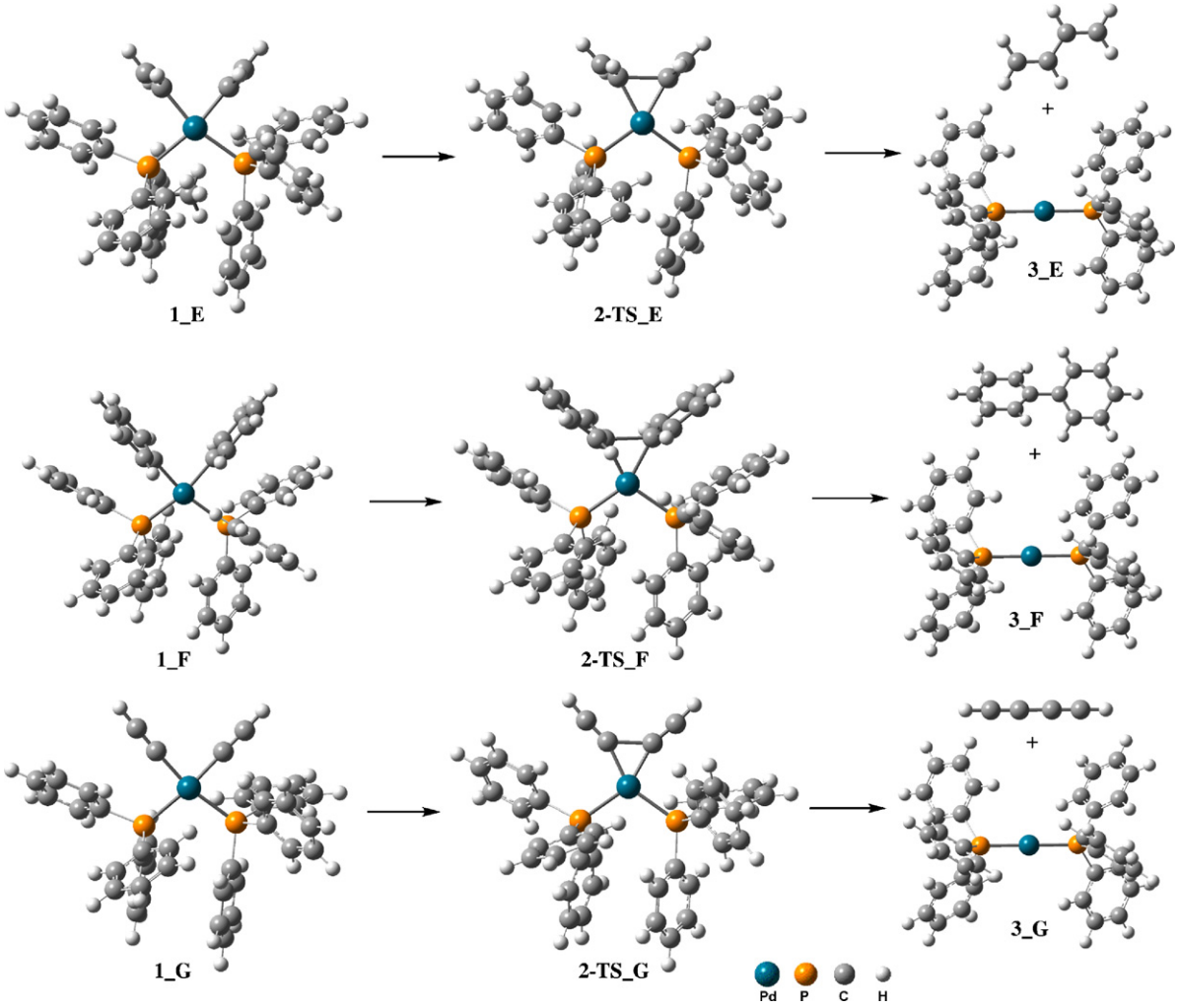

Fig. 5. ONIOM(B3LYP:HF) optimized structures of the initial complexes, transition states and products of the Me–Me coupling from the $[Pd(R)_2(PPh_3)_2]$ complexes: **1_E–3_E**: R=CH=CH_2; **1_F–3_F**: R=Ph; **1_G–3_G**: R=C≡CH; (see **1_C–3_C** in Fig. 4 for R=Me) [29,57].
© 2007 Wiley-VCH Verlag GmbH & Co. KGaA. Reproduced with permission.

to the molecular nitrogen formation and the mechanism of fragmentation process, which may involve singlet or triplet (diradical) species [63,64].

A theoretical study was carried out to understand the origins of enantioselectivity in homogeneous Cu-catalyzed enantioselective cyclopropanation reaction involving the chiral 8-oxazolinylquinoline ligand (Scheme 8) [65]. For this reaction eight possible transition states were calculated for each *cis*- and *trans*-

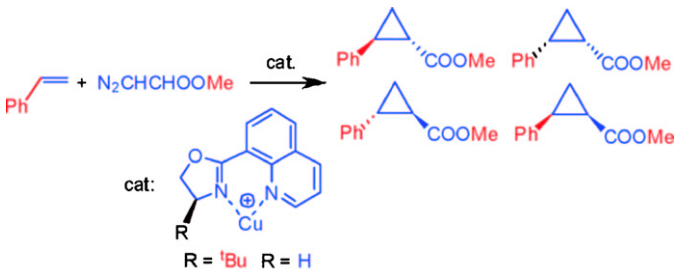

Scheme 8. ONIOM (B3LYP:UFF) partitioning scheme utilized in the theoretical study of Cu-catalyzed enantioselective cyclopropanation MM part – all Ph, Me and tBu groups (red color), QM part – the rest of the system (blue color) [65]. (For interpretation of the references to color in this scheme legend, the reader is referred to the web version of the article.)
© 2008 American Chemical Society. Reproduced with permission.

diastereomeric reaction channels and considering different relative dispositions of the reagents. It was found that lowest energy conformations were always associated with a far relative disposition of the specific groups in the reagents (the alkene and the carbonyl group in carbene moiety). In addition, steric interaction between the carbonyl oxygen and the group in 2-position of the quinoline ligand made an important contribution to favor one of the reaction channels. The fact is of interest, since it highlights the role of steric interactions, which are not originated from the stereogenic centers, but still contribute to the final enantioselectivity. For the studied reaction calculated *trans*-/*cis*-diastereoselectivities and enantioselectivites were in reliable agreement with experimental data [65]. A comparative B3LYP and ONIOM(B3LYP:UFF) study of another Cu-catalyzed cyclopropanation system has also successfully reproduced the experimental trends and have shown that overall enantioselectivity of the reaction depends on the balance of several different contributions from ligand/reactant orientations and steric repulsions [66].

As shown above investigation of the mechanism of asymmetric reactions involves analysis of several reaction channels leading to the final product. Usually a few transition states located manually are considered in the theoretical studies. However, the recent study on the Ru-catalyzed asymmetric hydrogenation using semi-automated systematic search of the potential energy surface with GRRM-ADD approach (see Section 2.6 for the method description)

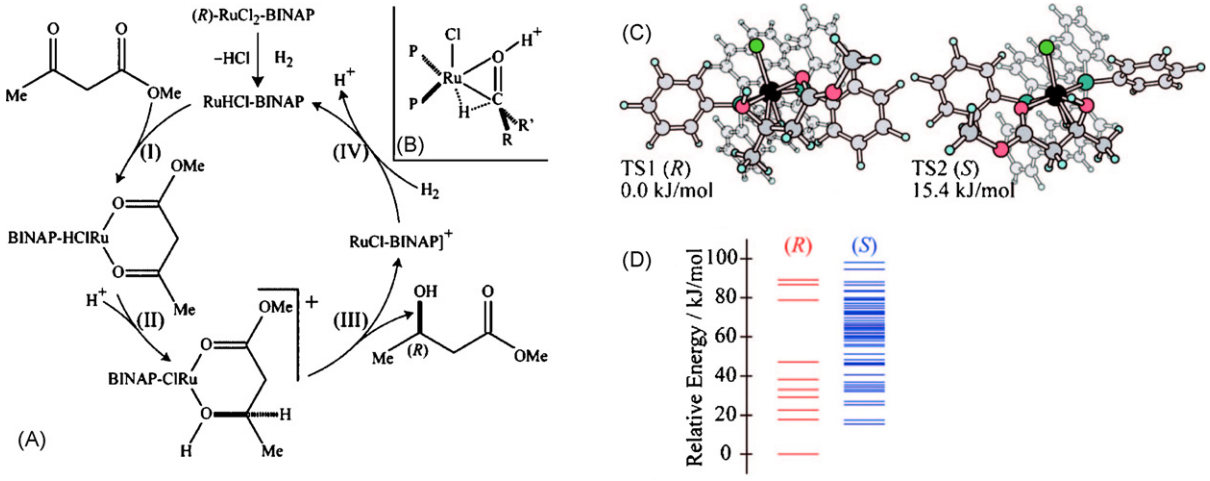

Scheme 9. (A) The mechanism of the Ru((*R*)-BINAP)-catalyzed asymmetric hydrogenation of methyl-3-oxobutanoate; (B) reaction center; (C) the lowest transition states leading of *R*-type (TS1) and *S*-type (TS2) products; (D) free energy distribution of the 10 *R*-type and 52 *S*-type transition states (<100 kJ mol^{-1}) [67].
© 2008 American Chemical Society. Reproduced with permission.

at the ONIOM(B3LYP:UFF) level has revealed much more complicated picture [67]. Numerous transition states were located for just one elementary step of the catalytic cycle (Scheme 9). The complexity of the system, appeared due to bulky ligands and several molecular arrangements in the complex, resulted in 62 transition states with the activation barrier below 100 kJ mol^{-1} (Scheme 9). For the lowest transition states TS1 and TS2 the calculated Boltzmann distribution of 143:1 clearly predicts the enantiomeric excess of >99% in favor of *R*-type product in total agreement with experimental findings [67]. The study has suggested that ester-oxygen coordination and carbonyl coordination direction at the reaction center are the microscopic origins of the selectivity (Scheme 9). Clearly, GRRM-ADD guided full search of the potential energy surface of elementary steps of the asymmetric reaction coupled with hybrid theoretical methods (QM:MM or QM:QM) offers essential advantage for the location of transition states, which can hardly be achieved with the same efficiency based on a typical manual procedure.

Another important studies carried out for the chiral transition–metal systems include investigation of stereochemical nonrigidity of Rh complexes [68], mechanism of asymmetric hydrogenation in [Rh((*R,R*)-Me-DuPHOS)]$^+$ catalyzed reaction [69,70], [Rh((*R*)-BINAP)]$^+$ catalyzed reaction [71], and other Rh systems [72].

The accuracy of the hybrid calculations in the studies of enantioselective reaction was evaluated for the Ti-catalyzed cyanation of benzaldehyde [73]. The theoretical predictions of stereoselectivity were found in reliable agreement with experimental data and linear relationship between the calculated and experimental $\Delta\Delta G^{\neq}$ values was found for the ligands with a single chiral center [73].

2.3. The influence of molecular environment on structure and reactivity of transition metal systems

Mechanistic studies carried out in recent years have suggested that dinuclear and polynuclear transition metal complexes and clusters play an important role in various catalytic transformations. Two types of processes responsible for *in situ* modification of the catalysts are of principle importance in this regard: (i) aggregation of metal species in solution to form large metal particles; and (ii) leaching of the metal atoms and clusters from the surface of nanoparticles. Both types of transformations were shown to dramatically affect a number of carbon-carbon bond-formation reactions [74–77]. Dimerization and polymerization of the metal complexes in solution was also of key-importance to maintain high catalyst activity in carbon–heteroatom bond formation [78–80]. These recent findings are in a sharp contrast with many generally accepted catalytic cycles related to homogeneous catalysis, which assume involvement of only mononuclear transition metal complexes. In the present section we discuss the questions related to the structure and reactivity of the complexes depending on the number of metal atoms present, as well as their structural organization.

The ONIOM(B3PW91:HF) study of self-aggregation of Ru complexes resulted in the dimerization energy of ΔE = 8–10 kcal mol^{-1}, which was in good qualitative agreement with experimentally measured ΔG values (quantitative comparison with experiment data was not possible, since it would require accurate calculation of entropy contribution in solution) [81]. The theoretical study of the dimerization process in conjunction with experimental NMR observation of aggregation in $CDCl_3$ solution indicated that the aggregates are relevant intermediates for the mechanism of transfer hydrogenation [81].

Formation of trinuclear complexes with Pt–Pt and Pt–Ag metal–metal bonds (Scheme 10) was studied and the steric effect of the phenyl groups was evaluated using the ONIOM(BLYP:UFF) approach [82]. The analysis of the reaction mechanism has shown that dissociative pathway takes place in the system resulting in formation of complex **2** with L = PPh_3, but leading to **2C** with 2L = acac (Scheme 10). Interestingly, the Ag^+ center interacts with Pt and P in **2**, and with two Pt atoms in **2C**. Complex **2** highlighted on the scheme was stable enough to be isolated and studied by X-ray technique [82].

The nature of the metal–metal bond is the key issue related to the electronic structure of the dinuclear and polynuclear species. Rather complicated case of "open-lantern-type" dinuclear Cr^{II} complexes was investigated with a series of theoretical methods (Fig. 6) [83]. In the DFT study the calculated energy decreases as the Cr–Cr distance becomes shorter and the equilibrium structure was not found. According to the ONIOM(CASSCF:DFT) calculations the energy increases as the Cr–Cr distance becomes shorter, but the equilibrium structure again was not found (Fig. 6C). In contrast, ONIOM(MRMP2:DFT) level did result in equilibrium structure at Cr–Cr distance 1.851 Å (the experimentally determined value was 1.960 Å) [83]. These calculations suggest that both non-dynamical and dynamical correlations are important in this system, and ONIOM approach provides flexible tool to apply desired computational level in the localized region of molecule.

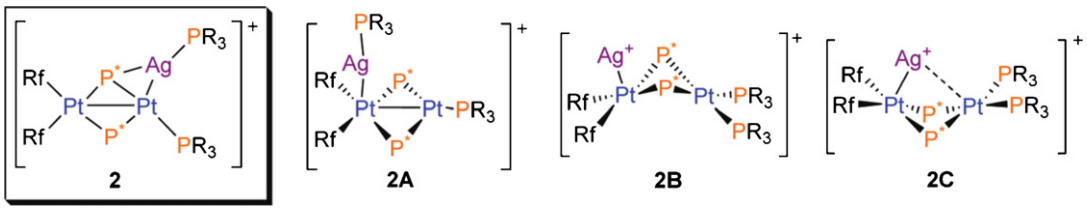

Scheme 10. Isomers of the trinuclear Pt_2Ag complexes studied by ONIOM calculations (P*=PR_2, Rf=C_6F_5, R=H, Ph; in **2C** bidentate acac ligand may be coordinated instead of two PR_3 ligands) [82].
© 2009 American Chemical Society. Reproduced with permission.

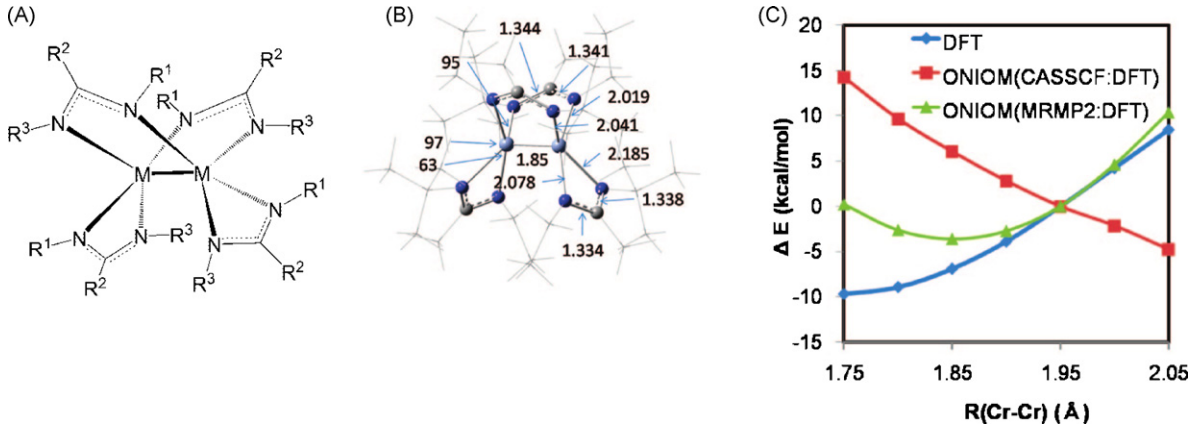

Fig. 6. (A) The structure of the dinuclear chromium complex (M=Cr, R^1=Et, R^2=Me, R^3=*t*Bu); (B) ONIOM partitioning and selected optimized geometry parameters (high-level part is shown in ball and sticks); (C) relative energy change depending on the metal–metal distance [83].

The dinuclear $Fe_2(CO)_6(PX)_2$ derivatives were reported to adopt different geometries and electronic states (tetrahedrane, "butterfly" diradical or planar rhombus) depending on the molecular environment of the complex and were correctly represented with hybrid calculations [84].

Dimerization of metal species (and formation of larger aggregates) in solution in some cases enhances chemical reactivity or catalytic activity, while in the other cases it is a pathway of deactivation. A good representative example of the latter for Mo-mediated nitrogen activation was reported in the ONIOM study [36]. It was shown that dimerization of catalytically active [Mo(NRPh)$_3$] complex to form [(NRPh)$_3$Mo≡Mo(NRPh)$_3$] dimer strongly depends on the ligand. For the smaller R groups the dimerization step is exothermic and provides strong driving force for this transformation, but in the case of larger peripheral ligands the dimerization step becomes endothermic [36]. When dimerization step involving the metal species is unlikely, nitrogen coordination and activation should proceed more efficiently. Experimental evidence of catalyst deactivation due to polymerization of metal species was also reported for catalytic C–X bond-formation reactions [78–80].

Theoretical calculations at the ONIOM(DFT:UFF) level were shown to provide reliable description for the other bimetallic systems involving the Ru–Sn and Os–Sn bonded structures [85].

Supramolecular organization of the metal species in solution is another important option to be considered in order to understand the reactivity of complexes and selectivity of chemical transformations. The studies of explicit interactions with solvent molecules provide the necessary information concerning stabilization of the metal species and availability of active sites to interact with reactants. A combination of hybrid QM:MM Car-Parinello and classical molecular dynamics simulations was carried out to investigate aqueous solvation of the $[Ru(bpy)_3]^{2+}$ cation [86]. The first hydration shell was found to involve ca. 15 water molecules in hydrogen bonded chains. The water molecules were intercalated between the bpy ligands and preserved highly dynamic structure with the characteristic water-exchange time of 12 ps [86]. Structure forming properties of the metal ions were demonstrated even in the second shell. Calculated mean residence time for the water molecules in the second shell of UO_2^{2+} and TiO^+ was 5.5 ps [87] and 3.6 ps [88], respectively, which was much higher than the value for pure water (1.7 ps). QM:MM molecular dynamics simulations were shown to provide appropriate description of the aggregates formation and their interaction with solvent molecules [89]. Theoretical molecular dynamics study of hydration of the Hg^I dimer has shown that about four ligands were bound to each of the mercury atoms in Hg_2^{2+} and the water molecules exchange took place in the picoseconds timescale [90]. A geometrical isomerization of less stable *cis*-diaquotriamminezinc(II) complex to a more stable *trans*-derivative was observed after 11.5 ps during the molecular dynamics simulations in aqueous solution at QM:MM level [91].

2.4. Modelling reactions on the surfaces

Reactions on the surface and heterogeneous catalysis (with supported and immobilized catalysts) are the area of active application of hybrid quantum chemical methods. Placing catalyst active site, some parts of the surface and the reactants into the higher layer with the rest of the surface presented into the lower layer makes it possible to get reliable mechanistic information at reasonable computational cost. As an example, deposition of the oxomanganese water oxidation catalyst on TiO_2 surface was modeled at ONIOM(B3LYP:UFF) level (Fig. 7) [92]. Binding of the manganese complex to the surface was characterized with calculated binding energy of $\Delta H = -54\,kcal\,mol^{-1}$ and resulted in several structure rearrangements in the metal complex. In these calculations the whole TiO_2 part was treated at the molecular mechanics level, thus, only steric effect from the support was taken into account [92].

More accurate representation of the supported systems may be achieved if some atoms of the support (at least those involved in

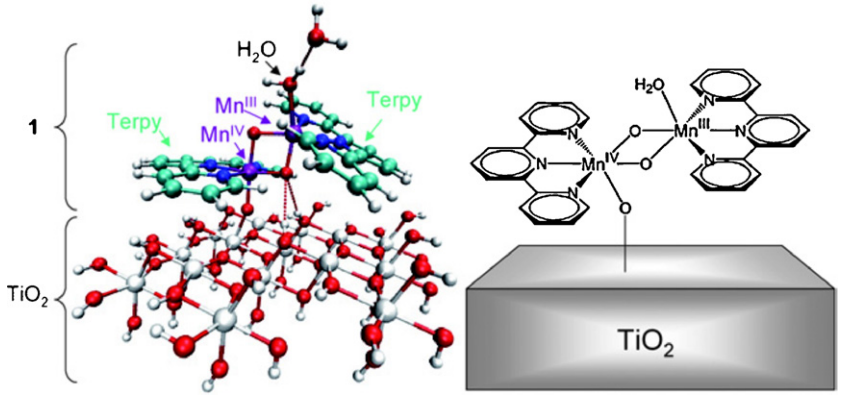

Fig. 7. Optimized geometry of the ONIOM(B3LYP:UFF) model of complex **1** anchored to TiO_2 (left) and the schematic representation of the model (right) [92].
© 2009 The Royal Society of Chemistry. Reproduced with permission.

the anchoring interaction) are also included in the higher layer. This type of ONIOM partitioning scheme was applied to study Pd_9 cluster anchored on a carbon nanotube and to investigate the reactivity towards molecular hydrogen (Fig. 8) [93,94]. Calculated interaction energy of the Pd_9 cluster and carbon nanotube was 86.8 kcal mol^{-1}, BSSE-correction with counterpoise method lowered the value to 54.3 kcal mol^{-1} [93].

The energy barriers for the H_2 activation on Pd_9/nanotube system were 2.4–3.0 kcal mol^{-1} (Fig. 8) [94]. If the carbon nanotube support was removed from the model, the barrier of hydrogen fragmentation on the isolated Pd_9 cluster was about 5.7 kcal mol^{-1}. The result indicates that hydrogen fragmentation should be easier in the presence of support. The authors have compared the next step – diffusion of atomic hydrogen – for the isolated metal cluster and supported cluster. In a similar way, the process was found to be easier in the case of supported Pd_9 cluster [94]. The study is related to the mechanism of hydrogen activation and catalytic hydrogenation reactions and it clearly indicates that isolated metal species are unrealistic models for the supported catalysts.

The above mentioned values of interaction energies are of similar magnitude as the ONIOM[MP4(SDQ):UFF] calculated binding energies in the $(H_3P)_2M$-C_{60} system: 47.5 and 38.7 kcal mol^{-1} for M = Pt and Pd, respectively [95]. The study also reported an important discussion concerning optimal partitioning scheme for the fullerene molecule. With correct system partitioning almost the same values were obtained at the ONIOM[MP4(SDQ):B3LYP] and ONIOM[MP4(SDQ):UFF] levels: 45.5 and 47.5 kcal mol^{-1}, respectively [95].

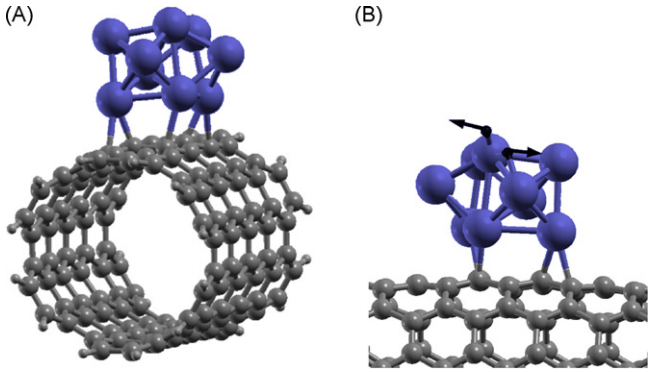

Fig. 8. (A) ONIOM (B3LYP:UFF) optimized structure of Pd_9 cluster anchored on the carbon nanotube; (B) transition state of hydrogen molecule fragmentation on the Pd_9 cluster supported on the carbon nanotube [94].
© 2009 The Royal Society of Chemistry. Reproduced with permission.

Grafting of the perhydrocarbonyl Os complex on a silica surface was shown to proceed through the σ-bond metathesis [96]. The process involved geometry change from distorted tetrahedral structure of bisalkylidene complex $[Os(=CH\mathit{t}Bu)_2(CH_2\mathit{t}Bu)_2]$ to "butterfly" structure of alkylidyne complex $[(\equiv SiO)Os(\equiv C\mathit{t}Bu)(CH_2\mathit{t}Bu)_2]$ [96].

Hybrid calculations have shown very impressive potential in understanding the mechanism of chemical transformations involving zeolites and various zeolite catalysts. The reliability of the application of QM:MM approach was investigated for the system with cobalt cationic sites in ferrierites [97]. QM:MM calculations were used to study adsorption of benzene to copper in CuHY zeolite [98], zeolite-supported Pd_4 clusters [99], interaction of CO with supported Au_{1-5} clusters [100], adsorption of Cu_{1-5} clusters [101], epoxidation of unsaturated hydrocarbons with H_2O_2 on the $TiSi_{64}O_{97}H_{74}$ nanocluster [102], and catalytic benzene hydroxylation over Fe-ZSM-5 zeolite [103].

The performance of hybrid calculations was evaluated for the models of H-FAU zeolites with 10 different combinations of two-layer ONIOM approach involving density functional, semi empirical, HF and MM levels [104]. The DFT:MM level was found to provide reliable description for the studied system. Calculated interaction energies of ethylene, benzene, and ethylbenzene were −8.7, −15.2, and −21.1 kcal mol^{-1} at ONIOM(B3LYP/6-311++G(d,p):UFF) level for the 84T cluster, which compare well with experimental values of −9.1, −15.3, and −19.6 kcal mol^{-1}, respectively. It was found that ONIOM(QM:MM) calculations on the larger system resulted in much more realistic description than full QM calculation on a small sized model. Unreliable interaction energies of −8.14, −7.48, and −7.76 kcal mol^{-1}, respectively, were calculated with a small 3T cluster at full B3LYP level. The study provided an excellent example of importance of the lattice framework surrounding in addition to the Brønsted group center [104].

Hybrid calculations were shown to provide reliable description of metal-organic framework systems. The examples of theoretical studies of molecular structures and interaction energies of MOF-5 [105] and IRMOF-1,2,3 [106] can be mentioned in this regard. The preliminary studies suggest that hybrid methods can provide reasonable description of molecular environment in the complex MOF structures.

2.5. Practical recommendations for application of ONIOM approach

The limitations of the ONIOM approach were discussed in details in the previous review articles [3,5,6]. Briefly, it was shown that upon application of the ONIOM calculations one should pay a

Table 1
Overview of the used ONIOM schemes in calculation of the different properties of transition metal complexes.

Calculations	High layer	Low layer	System[a]
Ligand geometry	B3LYP/Lanl2dz	UFF	Phosphine ligands [24,26], NHC ligands [27]
Metal complex structure	B3LYP/3-21G(d)	UFF	Ti^{IV}/Cu^{I} heteropolynuclear species [110]
	B3LYP/Lanl2dz	UFF	Pt/As ligand [112], Pd/As ligand [112]
	B3LYP/6-31G & Lanl2dz	UFF	Ir/salen [113]
	B3LYP/6-31G(d) & Lanl2dz	MM3 + UFF	Zinconocene derivatives [46]
	B3LYP/6-31G(d) & CEP-31G	UFF	Mo [114,115]
	B3LYP/D95 & Lanl2dz	UFF	Pd_9/carbon nanotube [93,94]
	B3LYP/6-31G(d,p) & Lanl2dz(f)	UFF	Pt_2Ag/phosphine [82]
	B3LYP/6-311G(d)	UFF	$Fe_2(CO)_6(PX)_2$ [84]
	B3LYP/6-311 + G(d)	UFF	Fe [118]
	B3PW91/6-31G(d) & Lanl2dz	UFF	Zr/(N,N,N) [116]
	B3PW91/6-31G(d,p) & SDD	UFF	Ru [119]
	B3PW91/6-31G(d,p) & SDD(f)	HF/4-31G & Lanl2dz	Ru/hydride [31]
	B3PW91/D95 & Lanl2dz	UFF	Ru–Sn [85], Os–Sn [85]
	CASSCF/cc-pVDZ & SDD	B3LYP	Cr^{II}/dinuclear complex [83]
	CASSCF/CEP-31G(d)	MM3	Cu/nitrene [108]
	MP4(SDQ)/6-31G & Lanl2dz	UFF	Pd/C_{60} [95], Pt/C_{60} [95]
	MP4(SDQ)/6-31G & Lanl2dz	B3LYP/6-31G & Lanl2dz	Pt/C_{60} [95]
	MRMP2/cc-pVDZ & SDD	B3LYP	Cr^{II}/dinuclear complex [83]
Reaction mechanism	HF/Lanl2dz & 6-311G(d,p) & STO-2G	MM3	Pt/phosphine [34,35]
	B3LYP/6-31G(d)	LSDA/Lanl2mb	Co/carbonyl [33]
	B3LYP/6-31G(d)	UFF	Co/carbonyl [33], Ni [44], Ni/diphosphine [64]
	B3LYP/6-31G(d) & Lanl2dz	HF/Lanl2mb	Pd/phosphine [60–62]
	B3LYP/6-31G(d) & SDD(f)	UFF	Rh/xanthene ligand [49]
	B3LYP/6-31G(d) &Lanl2dz	HF/3-21G & Lanl2dz	Mo/N ligands [36]
	B3LYP/6-31G(d,p) & Lanl2dz	HF/Lanl2mb	Ir/NHC [47], Ru/phosphine [55], Os/phosphine [55]
	B3LYP/6-31G(d,p) & Lanl2dz	UFF	Ti/Cp* [45]
	B3LYP/D95 & Lanl2dz	UFF	Pd_9/carbon nanotube [94]
	B3LYP/CEP-31G	HF/Lanl2mb	Zr/(P,N) [41]
	B3LYP/CEP-31G	UFF	Zr/(P,N) [41]
	B3LYP/6-311G(d) & SDD	B3LYP/Lanl2dz	Pd/phosphine [29]
	B3LYP/6-311G(d) & SDD	HF/Lanl2mb	Pd/phosphine [29]
	B3LYP/6-311G(d,p) & Lanl2dz	HF/Lanl2mb	Ru/phosphine [56]
	B3PW91/6-31G(d) & SDD(f)	UFF	Zr/(N,N,N) [63]
	B3PW91/6-31G(d,p) & SDD(f)	B3PW91/3-21G	Os/silica [96]
	B3PW91/6-31G(d,p) & SDD(f)	HF/4-31G & Lanl2dz	Ru [81]
	B3PW91/6-31G(d,p) & SDD(f)	HF/4-31G & Lanl2dz	Ti/imido alkyl complex [52]
	BHandH/6-31G(d) & Lanl2dz	UFF	Ir/Tp′ [48], Ir/Tp′ [51]
	BP86/6-31G(d,p) & SDD	HF/Lanl2mb & 6–31G	Ru/NHC [28],
	BP86/tz + p & dz + p	Sybyl/TRIPOS MM	Zr/zirconocene [53], Pd/phosphine [124]
	PW91/D95 & Lanl2dz	UFF	Mn/porphyrin [50]
	TPSS/6-31G(d) & Lanl2dz	UFF	Ti [54]
	CCSD(T)/6-31G(d) &Lanl2dz	B3LYP/6–31 + G(d,p) & Lanl2dz	Mo/N ligands [36]
	MP2/6-31G(d) & SVP	HF/3-21G	Zn [43]
Modeling of surfaces and complex frameworks	MP2/6-31G(d,p)	HF/6-31G(d,p)	MOF-5 [105]
	HF/6-31G	PM3	IRMOF-1,2,3 [106]
	B3LYP/dz	UFF	Mn/TiO_2 [92]
	BP86/tzvp & cc-pVTZ-PP	Gulp-MM	Cu/zeolite [98]
	B3LYP/tzvp & cc-pVTZ-PP	Gulp-MM	Cu/zeolite [98]
	B3LYP/6-31G(d,p) & Lanl2dz	UFF	Pd_4/zeolite [99], TS-1 [102]
	BPW91/D95 & Lanl2dz	UFF	Au_{1-4}/zeolite [100], Cu_{1-4}/zeolite [101]
	B3LYP/D95(d,p) & Lanl2dz	UFF	Fe-ZSM-5 [103]
	BPW91/6-311 + G(d,p) & Lanl2dz	UFF	Au_{1-4}/zeolite [100], Cu_{1-4}/zeolite [101]
	B3LYP/6-311 + +G(d,p)[b]	UFF[b]	H-FAU zeolite [104]
Enantioselective reactions	B3LYP/6-31G(d)	UFF	Cu/quinoline [65]
	B3LYP/6-31G(d)	HF/STO-3G	Ti [73]
	B3LYP/6-31G(d) & Lanl2dz	UFF	Cu [66]
	B3LYP/Lanl2dz	HF/Lanl2mb:UFF[c]	Rh/phosphine [69,70]
	B3LYP/D95(d) & Lanl2dz	MM3	Rh/phosphine [71]
	B3LYP/6-311 + +G(d,p), 6-31G(d) & Lanl2dz(f)	UFF	Ru/phosphine [67]
	B3PW91/6-31G(d,p) & SDD	UFF	Rh/phosphine [68]

[a] Details of structures of the used ligands and reactants are omitted for clarity.
[b] Several other levels were also studied, see the provided reference for more details.
[c] Three-layers were considered within the ONIOM approach.

special attention: (a) to the partitioning of the system under investigation, (b) to the choice of high-level and low-level methods for the "model" and "real" parts of the system, (c) to the use of electronic and mechanical embedding techniques, (d) to evaluate the S-value test, and more [3,5,6]. In this review, we will not repeat these well-analyzed aspects of the ONIOM, but will present a few examples that clearly demonstrate these points of review, and outline a best strategy in the use of ONIOM technique.

At first, let us mention, once again, that the chosen high-level and low-level methods in ONIOM should be applicable to the "model" and "real" systems. In Table 1, we summarize the widely used combinations of the high-level and low-level methods in the

literature to study chemistry of the transition–metal systems. As we can see from this table, the majority of these approaches use the popular DFT methods as a high-level (or as a QM-level) approach, while the application of other quantum chemical methods, such as CCSD(T), MP2, MP4 and CASSCF, was also reported. The molecular mechanics method at the UFF level and the HF method with the small basis sets were utilized most frequently as low-level methods. However, as it was demonstrated in several theoretical studies that popular DFT approach may not be applicable to specific problems of certain transition–metal systems [11]. Therefore, one should be very careful in use of DFT, in general, and some specific density functionals, in particular, as a high-level method in ONIOM.

Indeed, it was demonstrated that the use of DFT and other QM methods in ONIOM(QM:MM) for the transition metal systems with C–H···π-stacking interactions may lead to rather large differences in the calculated energetic of the system [68]. This was a result of poor performance of the conventional DFT approaches in describing of the weak C–H···π-stacking interactions compared with CCSD(T) or MP2 techniques. It was reported the better agreement between the calculated and experimental values of the energy barriers was obtained only after applying the MPW2PLYP functional, which includes MP2 correction, as a high-level method in ONIOM [68]. The performance of the ONIOM calculations to describe the systems with H-bonding interactions was also discussed [107].

Similarly, the DFT and CASSCF methods were shown to provide different description of the lower-lying electronic states of the Cu/nitrene system; relatively inexpensive DFT calculations indicated that a triplet was a ground state, while the expensive CASSCF calculations resulted in a singlet ground state [108]. Flexible nature of the hybrid approaches allows to apply CASSCF technique as a high-level method in ONIOM to study the real-sized system and evaluate all possible effects on the relative stability of the lower-lying electronic states of this system [108].

Single point energy calculations (at the ONIOM (BLYP:UFF) optimized geometries) of Pt complexes at the LMP2 and M06 levels [109] were resulted in up to 20 kcal mol^{-1} difference with ONIOM (BLYP:UFF) energies [82].

Meantime, ONIOM (B3LYP/3-21G(d):UFF) approach was reported to provide acceptable geometry for Ti^{IV}/Cu^{I} heteropolynuclear species [110]. In spite of computational efficiency of such small basis set, it cannot be recommended to use extensively without being carefully evaluated for the given transition metal systems.

A failure of the ONIOM (B3LYP:UFF) method to locate some of the transition states was reported for the Rh-catalyzed hydroacylation reaction [111]. Here, the applicability of the used B3LYP and UFF methods and utilized partitioning scheme of the entire system are the first things to be checked.

Next, we would like to discuss the reliability of hybrid calculations related to the metal-containing systems. The comparison of the X-ray and calculated geometry parameters by the hybrid methods was reported for the Pt [29], Ir [47], Ni [64], Pt [82], Ru [81,119], Mo [117], Fe [118], complexes and several other systems. Generally, with the correct choice of the partitioning scheme and reliable theory levels the hybrid approach provides a good agreement between the calculated and X-ray structural data. Noteworthy, the ONIOM approach was successfully utilized to refine the experimental data, since results of X-ray analysis left unanswered several structural motives of the system [118–120].

Conformational flexibility of the ligands should be taken into account when comparison of optimized and experimentally determined geometries is carried out. For example, different orientations of Ph and Cy groups in the PPh_3 and PCy_3 ligands may have a similar effect on geometry as the ligand effect. These observations were confirmed by X-ray studies for the metal complexes crystallized in different conformations [29].

Table 2
Activation ($\Delta E^{\neq}$) and reaction (ΔE) energies (in kcal mol^{-1}) of the C–C coupling reactions (**1** → **2-TS** → **3**)[a] calculated at the ONIOM(B3LYP/BSI:B3LYP/Lanl2dz)[b] (A), ONIOM(B3LYP/BSI:B3LYP/Lanl2dz)//ONIOM(B3LYP/BSI:HF/Lanl2mb) (B) and ONIOM(B3LYP/BSI:HF/Lanl2mb) (C) levels of theory [29].

No.	Initial complex 1	$\Delta E^{\neq}/\Delta E$[c]		
		A	B	C
1	$Pd(PPh_3)_2(CH_3)_2$	22.5/−38.4	23.1/−39.2	23.9/−34.5
2	$Pd(PPh_3)_2(CH{=}CH_2)_2$	3.9/−41.9	3.7/−44.2	5.3/−36.8
3	$Pd(PPh_3)_2Ph_2$	7.8/−42.4	9.7/−43.2	11.4/−35.2
4	$Pd(PPh_3)_2(C{\equiv}CH)_2$	13.0/−23.3	13.3/−24.1	15.3/−16.2

[a] The C–C coupling reaction and partitioning scheme are shown in Scheme 2 (L = PPh_3).
[b] BSI corresponds to a combination of 6-311G(d) and SDD bases sets.
[c] The $\Delta E^{\neq}$ and ΔE values for each case are given before and after the slash symbol, respectively.

In some cases ONIOM calculated geometries of the complexes and transition states were used as starting points for full QM investigations [48,121,122]. Such strategy is advisable if a systematic search and evaluation of several isomers and reaction pathways have to be performed at computationally expensive QM level [123].

The choice of the low-level method in the ONIOM studies is as important as the choice of the high-level approach, discussed above. As seen in Table 1, in majority of ONIOM schemes used for transition metal system the various MM approaches were utilized as a low-level approach. Although the use of MM methods in these calculations was helpful to analyze steric effects, purely molecular mechanics treatment may lead to wrong description of the reaction energies, as well as the reaction pathways, because of lack of possible electronic effects from the "real" part of the system [124]. Furthermore, one should pay a special attention to electronic and mechanical embedding schemes in the QM:MM approach [3–9].

One of the ways to enhance the predictive power of ONIOM approach and overcome deficiency of the adopted MM methods as a low-level method, is the single point QM calculations of the entire system at the ONIOM (QM:MM)-optimized geometries. Such strategy was successfully applied to study Ir [47,51], Ti [52,73], Zn [43], Ru [28], Pd [29,93], and Os [96] complexes and several other systems. Often for the single point calculations the same level was utilized as for the higher layer in the ONIOM calculations.

Another strategy is the use of the HF method with a small basis set or a semiempirical SCF method as a low-level method in ONIOM studies. This strategy was proven to be reliable in the study of a series of C–C coupling reactions, **1** → **2-TS** → **3**, calculated on Pd complexes (see Scheme 3 and Table 2) [29]. Potential energy surface of these reactions were calculated at the three different level of theory: ONIOM(B3LYP/BSI:B3LYP/Lanl2dz) level (A), ONIOM(B3LYP/BSI:B3LYP/Lanl2dz)//ONIOM(B3LYP/BSI:HF/Lanl2mb) level (B) and ONIOM(B3LYP/BSI:HF/Lanl2mb) level (C). It was found that approaches A [with low-level = B3LYP/Lanl2dz for geometry optimization] and C [with low-level = HF/Lanl2mb for geometry optimization] provide similar results. While approach B, i.e. single point ONIOM (B3LYP/BSI:B3LYP/Lanl2dz) calculation at the ONIOM (B3LYP/BSI:HF/Lanl2mb) optimized geometries, improves significantly the energetics of the reaction compared to the level C. Thus, geometry optimization at the ONIOM(B3LYP/BSI:HF/Lanl2mb) level and single point energy calculations at the ONIOM(B3LYP/BSI:B3LYP/Lanl2dz) level could be a better strategy to obtain a reliable description of energies of the studied reactions at low computational costs.

ONIOM method in combination with PCM approach, called as an ONIOM-PCM, can be utilized to study media effect to the calculated properties of the transition metal systems [125] or to apply

ONIOM-PCM calculations and QM:MM molecular dynamics simulations [86]. More simplified approach involves single point PCM calculations using ONIOM optimized geometry [28,50,73,82].

It is well established that one should pay a special attention to the charged species. If the charge of the metal complex under investigation changes during the reaction, gas-phase and solution phase studies may result in 20–50 kcal mol^{-1} difference in the calculated energies [126]. If the formal change of the metal complex under investigation does not change during the reaction, the difference in the gas-phase and solution phase calculated energies could be within ~10 kcal mol^{-1}, as it was shown for the reaction involving anionic zerovalent Pd and Pt species [127].

The reliable performance of the hybrid computational approach to study solution state structures and their relative stability was reported by comparing theoretical calculations with NMR experiments in solution employing NMR diffusion measurements, EXSY experiments and nuclear Overhauser effect measurements [68,81,82,107].

To summarize, the above-presented examples clearly demonstrate the importance of the choice of high-level and low-level methods in the ONIOM approach. It is advisable to test high-level method for the model system before using it as a high-level method in ONIOM scheme, most preferably using the S-value test. Similarly, it is of utmost importance to test low-level method for the real system (or part of that) before using it as a high-level method in ONIOM scheme. Considering rapid development of computational performance and increasing availability of multi-CPU systems, we anticipate frequent usage of more accurate quantum mechanical methods in addition to popular DFT calculations (at least in the high layer).

2.6. Brief review on some new developments in hybrid calculation methodology

In this part of the review we briefly highlight new algorithms and method developments in the area of hybrid calculations, which may find potential application in the nearest future to solve important chemical problems. The literature considered is limited only to the time period covered in the present review and reflects very recent trends. More comprehensive description on the numerical algorithms and theoretical approaches is available in the previous reviews [3–6,16–21].

The global reaction route mapping (GRRM) method based on anharmonic downward distortions (ADD) transition state (TS) search algorithm has been a very powerful tool for searching all (if necessary) TSs and intermediates systematically. It uses the ADD to find a TS from a local minimum and the intrinsic reaction coordinate (IRC) to find a local minimum from a TS and repeat this cycle until exhausted [128]. This method has successfully been applied to find all transition states for eight possible stereospecific pathways in the [$RuCl_2$-((*R*)-BINAP)]-catalyzed asymmetric hydrogenation (see Section 2.2) [67]. The original GRRM method is exhaustive but quite computer-time demanding for large molecular systems. Several options for less exhaustive search have been developed. One of them combines the GRRM method with the micro-iteration technique, in which the region directly not involved in reaction can be excluded from the TS search and is very convenient for TS search in combination with the ONIOM method [129]. The advantage of ADD calculations is to find out reaction channels automatically, excluding from consideration the regions which are not related to reaction pathways.

The other method development to deal with asymmetric reactions includes the Q2MM force field and its application for studying rhodium catalyzed asymmetric hydrogenation of enamides [130,131].

The performance of the large-scale parallel QM:MM calculations with coupled cluster formalism applied in the high level was evaluated for hydrated zinc-porphyrin system (30 Å box with 869 water molecules) [132]. A good scalability with the factors of 1.92 and 1.94 was observed for 256–512 CPUs, somewhat lower speedup values of 1.66 and 1.74 were found for 512–1024 CPUs [132]. Novel QM:MM molecular dynamics approach was utilized to investigate microsolvation of the zinc ion in aqueous solution [133]. In the developed model the overall system was partitioned into the QM region of variable size and a remaining MM region. Within this model even computationally inexpensive DFT method provided very good agreement with experimental data [133].

The performance of DFTB as low level quantum mechanical layer was evaluated within the two-layer ONIOM method [134–136]. The ONIOM(DFT:DFTB) combination was reported as good choice with an inexpensive low level method.

A two-layer ONIOM(QM:MM) calculations on PR_3 ligands, followed by molecular electrostatic potential analysis were suggested as a simple and useful method for evaluating the steric effect of the phosphine ligand [137]. The scope and the limitations of this approach were discussed in the literature [138–141].

Improved capping potentials for hybrid QM:MM calculations were developed to produce more accurate NMR chemical shifts [142]. A combination of molecular dynamics simulations and two-layer ONIOM method was used to calculate ^{1}H NMR chemical shifts in solution using the GIAO approximation [143]. Modified carbon pseudopotential for ONIOM calculations of metallocenes was proposed and showed to increase the accuracy in the calculations of stretching frequencies [144]. Within the ONIOM framework a QM:QM electronic embedding scheme based on Mulliken atomic charges to define the embedding potential was described [145,146]. Accurate bond dissociation enthalpies were predicted by the ONIOM-G3B3 method [147]. A possibility to improve the efficiency and accuracy of QM:MM calculations in prediction of physicochemical properties of molecular systems was discussed [148].

Several approaches are under development to compute free energy surfaces. A QM:MM minimum free energy path (QM:MM-MFEP) method was developed to calculate the free energies of large systems in solution with enhanced efficiency [149]. A combination of the QM:MM method with the theory of energy representation (QM:MM-ER) was reported to compute free energy change for chemical reactions in condensed phases [150]. Some other methods to deal with efficient and accurate free energy calculations have also been published recently [151–155]. A method for generation of potential energy function in the presence of an electrostatic potential was developed aimed to model chemical reactions in solution, in an enzyme, nanocavity, or other chemical environment [156].

3. Summary

According to recent experimental studies in many cases the metal complex added to the catalytic reaction can be considered only as a catalyst precursor. The actual catalyst is formed in reaction media upon interaction with reactants, solvents, etc., and the structure of the actual catalyst can be quite different from the precursor. Theory may have to decide what is actually reacting. We believe that theoretical chemists should accept this challenge and contribute to better understanding of catalytic reactions in the way only theory can provide.

To this end a new area of computational research should be developed dealing with *in situ* formed aggregates, clusters and supramolecular structures involving metal species. Formation of aggregates and clusters may enhance the reactivity. At the same time, there are well-established examples where dimerization or polymerization of metal species can also result in catalyst deactivation. Clearly, a dual role of transition metal complexes dimerization

(aggregation) should be further characterized in more details. Considering large size and increasing complexity of such systems hybrid theoretical approaches should be the methods of choice for the computational studies.

Although some theoretical studies have been carried out to elucidate the origins of enantioselectivity at the most fundamental level, considering the importance of this subject, more theoretical studies should be focused on this topic. The scope and reliability of the hybrid calculations discussed in the present review allows to elaborate subtle differences in the structure and energy of different transition states leading to different enantioselective products. In the advent of new TS search methods like GRRM, it is now becoming possible to systematically find and compare all the possible enantioselective transition states in complex transition–metal-catalyzed reactions.

Dynamical effects of the ligand environment and the reactant substituents may significantly affect the reactivity of the metal complexes and selectivity of chemical transformations. We believe that MD simulations will provide new insights into fundamental understanding of catalytic reactions. In the MD simulations the real-size molecules need to be considered for correct representation of the environment. Since a massive amount of calculations is required in MD runs, the ONIOM or other hybrid methods are the methods of choice and one has to pay attention to careful selection of layers and theory levels.

We end our brief review article by summarizing the three challenges in modern transition metal chemistry and catalysis which need to be studied rigorously in the coming years: (i) actual metal species, aggregates, clusters, supported catalysts and particles that really exist and play role in the reactions, rather than simple mononuclear classic models; (ii) dynamic nature of the catalytic reactions in addition to the static structures and activation barriers; and (iii) the detailed mechanism of enantioselective reactions and the origins of enantioselectivity.

References

[1] (a) F. Maseras, K. Morokuma, J. Comput. Chem. 16 (1995) 1170–1179; (b) M. Svensson, S. Humbel, R.D.J. Froese, T. Matsubara, S. Sieber, K. Morokuma, J. Phys. Chem. 100 (1996) 19357–19363; (c) S. Dapprich, I. Komáromi, K.S. Byun, K. Morokuma, M.J. Frisch, J. Mol. Struct.: THEOCHEM 461–462 (1999) 1–21.
[2] T. Matsubara, F. Maseras, N. Koga, K. Morokuma, J. Phys. Chem. 100 (1996) 2573–2580.
[3] T. Vreven, K. Morokuma, Ann. Rep. Comput. Chem. 2 (2006) 35–51.
[4] H. Lin, D.G. Truhlar, Theor. Chem. Acc. 117 (2007) 185–199.
[5] K. Morokuma, Proc. Jpn. Acad., Ser. B 85 (2009) 167–182.
[6] K. Morokuma, Bull. Chem. Soc. Jpn. 80 (2007) 2247–2261.
[7] D.G. Musaev, K. Morokuma, Top. Organomet. Chem. 12 (2005) 1–30.
[8] G. Ujaque, F. Maseras, Struct Bond. 112 (2004) 117–149.
[9] F. Maseras, Top. Organomet. Chem. 4 (1999) 165–191.
[10] A. Dedieu, Top. Organomet. Chem. 4 (1999) 69–107.
[11] C.J. Cramer, D.G. Truhlar, Phys. Chem. Chem. Phys. 11 (2009) 10757–10816.
[12] C. Bo, F. Maseras, Dalton Trans. (2008) 2911–2919.
[13] F.P. Rotzinger, Chem. Rev. 105 (2005) 2003–2037.
[14] J.N. Harvey, V.K. Aggarwal, C.M. Bathelt, J.-L. Carreón-Macedo, T. Gallagher, N. Holzmann, A.J. Mulholland, R. Robiette, J. Phys. Org. Chem. 19 (2006) 608–615.
[15] M. Sierka, J. Sauer, in: S. Yip (Ed.), Handbook of Materials Modeling, Springer, 2005, pp. 241–258.
[16] M. Bühl, Ann. Rep. NMR Spectrosc. 64 (2008) 77–126.
[17] A. Lodola, C.J. Woods, A.J. Mulholland, Ann. Rep. Comput. Chem. 4 (2008) 155–169.
[18] M. Lundberg, K. Morokuma, in: D.M. York, T.-S. Lee (Eds.), Multi-scale Quantum Models for Biocatalysis, Springer Science and Business Media B.V., 2009, pp. 21–55.
[19] H.M. Senn, W. Thiel, Curr. Opin. Chem. Biol. 11 (2007) 182–187.
[20] H.M. Senn, W. Thiel, Top. Curr. Chem. 268 (2007) 173–290.
[21] P.B. Karadakov, Annu. Rep. Prog. Chem., Sect. C 97 (2001) 61–90.
[22] V.P. Ananikov, L.L. Khemchyan, I.P. Beletskaya, Synlett (2009) 2375–2381.
[23] S.P. Nolan, O. Navarro, in: D.M.P. Mingos, R.H. Crabtree (Eds.), Comprehensive Organometallic Chemistry III, vol. 11, Elsevier Ltd., Oxford, 2007, pp. 1–37.
[24] T. Fujihara, S. Yoshida, J. Terao, Y. Tsuji, Org. Lett. 11 (2009) 2121–2124.
[25] R. Martin, S.L. Buchwald, Acc. Chem. Res. 41 (2008) 1461–1473.
[26] T. Fujihara, S. Yoshida, H. Ohta, Y. Tsuji, Angew. Chem., Int. Ed. 120 (2008) 8310–8314.
[27] H. Ohta, T. Fujihara, Y. Tsuji, Dalton Trans. (2008) 379–385.
[28] R.A. Diggle, S.A. Macgregor, M.K. Whittlesey, Organometallics 27 (2008) 617–625.
[29] V.P. Ananikov, D.G. Musaev, K. Morokuma, Eur. J. Inorg. Chem. (2007) 5390–5399.
[30] Under experimental conditions these pathways may be switched by addition of an excess of phosphine ligand (to retard ligand dissociation from the Pd complex and favour four-coordinated pathway) or by using low-ligated palladium species (to facilitate three-coordinated pathway). See Ref. [29] for discussion.
[31] Y. Gloaguen, G. Alcaraz, A.-F. Pécharman, E. Clot, L. Vendier, S. Sabo-Etienne, Angew. Chem. Int. Ed. 121 (2009) 2964–2968.
[32] N. Ungvári, E. Fördős, T. Kégl, F. Ungváry, Inorg. Chim. Acta 362 (2009) 1333–1342.
[33] E. Fördős, N. Ungvári, T. Kégl, L. Párkányi, G. Szalontai, F. Ungváry, Inorg. Chim. Acta 361 (2008) 1832–1842.
[34] T. Matsubara, J. Phys. Chem. A 112 (2008) 9886–9894.
[35] T. Matsubara, J. Phys. Chem. A 113 (2009) 3227–3236.
[36] N.J. Brookes, D.C. Graham, G. Christian, R. Stranger, B.F. Yates, J. Comput. Chem. 30 (2009) 2146–2156.
[37] D.G. Musaev, P. Babadova-Parvanova, K. Morokuma, Computational Modeling for Homogeneous and Enzymatic Catalysis: A Knowledge-Base for Designing Efficient Catalysts, Wiley-VCH Verlag GmbH & Co. KGaA, Weinheim, 2008, pp. 83–108.
[38] Q. Cui, D.G. Musaev, M. Svensson, S. Sieber, K. Morokuma, J. Am. Chem. Soc. 117 (1995) 12366–12367.
[39] D.C. Graham, G.J.O. Beran, M. Head-Gordon, G. Christian, R. Stranger, B.F. Yates, J. Phys. Chem. A 109 (2005) 6762–6772.
[40] R. Stranger, B.F. Yates, Chem. Phys. 324 (2006) 202–209.
[41] B.F. Yates, H. Basch, D.G. Musaev, K. Morokuma, J. Chem. Theory Comput. 2 (2006) 1298–1316.
[42] H. Basch, D.G. Musaev, K. Morokuma, J. Am. Chem. Soc. 121 (1999) 5754–5761.
[43] M. Uchiyama, Y. Kobayashi, T. Furuyama, S. Nakamura, Y. Kajihara, T. Miyoshi, T. Sakamoto, Y. Kondo, K. Morokuma, J. Am. Chem. Soc. 130 (2008) 472–480.
[44] T.R. Cundari, J.O.C. Jimenez-Halla, G.R. Morello, S. Vaddadi, J. Am. Chem. Soc. 130 (2008) 13051–13058.
[45] J.J. Carbó, O. González-del Moral, A. Martín, M. Mena, J.-M. Poblet, C. Santamaría, Chem. Eur. J. 14 (2008) 7930–7938.
[46] R. Fernández, A. Grirrane, I. Resa, A. Rodríguez, E. Carmona, E. Álvarez, E. Gutiérrez-Puebla, Á. Monge, J.M. López del Amo, H.-H. Limbach, A. Lledós, F. Maseras, D. del Río, Chem. Eur. J. 15 (2009) 924–935.
[47] C.Y. Tang, W. Smith, D. Vidovic, A.L. Thompson, A.B. Chaplin, S. Aldridge, Organometallics 28 (2009) 3059–3066.
[48] P. Lara, M. Paneque, M.L. Poveda, L.L. Santos, J.E.V. Valpuesta, E. Carmona, S. Moncho, G. Ujaque, A. Lledós, E. Àlvarez, K. Mereiter, Chem. Eur. J. 15 (2009) 9034–9045.
[49] M.À. Carvajal, S. Kozuch, S. Shaik, Organometallics 28 (2009) 3656–3665.
[50] M.C. Curet-Arana, G.A. Emberger, L.J. Broadbelt, R.Q. Snurr, J. Mol. Catal. A: Chem. 285 (2008) 120–127.
[51] P. Lara, J. López-Serrano, C. Maya, M. Paneque, M.L. Poveda, L.J. Sánchez, J.E.V. Valpuesta, E. Carmona, Organometallics 28 (2009) 4649–4651.
[52] M. Feliz, P.D. Bolton, P. Mountford, E. Clot, Organometallics 27 (2008) 6111–6122.
[53] D. Wang, S. Tomasi, A. Razavi, T. Ziegler, Organometallics 27 (2008) 2861–2867.
[54] Z. Flisak, Macromolecules 41 (2008) 6920–6924.
[55] T. Bai, J. Zhu, P. Xue, H.H.-Y. Sung, I.D. Williams, S. Ma, Z. Lin, G. Jia, Organometallics 26 (2007) 5581–5589.
[56] L. Zhang, L. Dang, T.B. Wen, H.H.-Y. Sung, I.D. Williams, Z. Lin, G. Jia, Organometallics 26 (2007) 2849–2860.
[57] V.P. Ananikov, D.G. Musaev, K. Morokuma, Computational Modeling for Homogeneous and Enzymatic Catalysis: A Knowledge-Base for Designing Efficient Catalysts, Wiley-VCH Verlag GmbH & Co. KGaA, Weinheim, 2008, pp. 131–148.
[58] V.P. Ananikov, D.G. Musaev, K. Morokuma, Organometallics 24 (2005) 715–723.
[59] L. Xue, Z. Lin, Chem. Soc. Rev., 2010, ASAP. doi:10.1039/b814973a (available on the web site).
[60] W. Zheng, A. Ariafard, Z. Lin, Organometallics 27 (2008) 246–253.
[61] A. Ariafard, Z. Lin, Organometallics 25 (2006) 4030–4033.
[62] A. Ariafard, Z. Lin, J. Am. Chem. Soc. 128 (2006) 13010–13016.
[63] T. Gehrmann, J.L. Fillol, H. Wadepohl, L.H. Gade, Angew. Chem. Int. Ed. 121 (2009) 2152–2156.
[64] T.R. Cundari, G.R. Morello, J. Org. Chem. 74 (2009) 5711–5714.
[65] J.M. Fraile, J.I. García, G. Jiménez-Osés, J.A. Mayoral, M. Roldán, Organometallics 27 (2008) 2246–2251.
[66] G. Drudis-Solé, F. Maseras, A. Lledós, A. Vallribera, M. Moreno-Mañas, Eur. J. Org. Chem. (2008) 5614–5621.
[67] S. Maeda, K. Ohno, J. Am. Chem. Soc. 130 (2008) 17228–17229.
[68] M.V. Câmpian, E. Clot, O. Eisenstein, U. Helmstedt, N. Jasim, R.N. Perutz, A.C. Whitwood, D. Williamson, J. Am. Chem. Soc. 130 (2008) 4375–4385.
[69] C.R. Landis, S. Feldgus, Angew. Chem., Int. Ed. 39 (2000) 2863–2866.
[70] S. Feldgus, C.R. Landis, J. Am. Chem. Soc. 122 (2000) 12714–12727.
[71] S. Mori, T. Vreven, K. Morokuma, Chem. Asian J. 1 (2006) 391–403.
[72] G.J. Gainsford, A. Falshaw, C. Lensink, M. Seth, Polyhedron 27 (2008) 2529–2538.

[73] S. Qin, C. Hu, H. Yang, Z. Su, D. Tang, J. Org. Chem. 73 (2008) 4840–4847.
[74] L.D. Pachon, G. Rothenberg, Appl. Organometal. Chem. 22 (2008) 288–299.
[75] N.T.S. Phan, M.V.D. Sluys, C.W. Jones, Adv. Synth. Catal. 348 (2006) 609–679.
[76] R. Narayanan, C. Tabor, M.A. El-Sayed, Top. Catal. 48 (2008) 60–74.
[77] J.G. de Vries, Dalton Trans. (2006) 421–429.
[78] V.P. Ananikov, K.A. Gayduk, I.P. Beletskaya, V.N. Khrustalev, M.Yu. Antipin, Eur. J. Inorg. Chem. (2009) 1149–1161.
[79] I.P. Beletskaya, V.P. Ananikov, Eur. J. Org. Chem. (2007) 3431–3444.
[80] V.P. Ananikov, I.P. Beletskaya, G.G. Aleksandrov, I.L. Eremenko, Organometallics 22 (2003) 1414–1421.
[81] G. Ciancaleoni, C. Zuccaccia, D. Zuccaccia, E. Clot, A. Macchioni, Organometallics 28 (2009) 960–967.
[82] E. Alonso, J. Forniés, C. Fortuño, A. Lledós, A. Martín, A. Nova, Inorg. Chem. 48 (2009) 7679–7690.
[83] Y.I. Kurokawa, Y. Nakao, S. Sakaki, J. Phys. Chem. A 113 (2009) 3202–3209.
[84] I. Silaghi-Dumitrescu, T.E. Bitterwolf, R.B. King, J. Am. Chem. Soc. 130 (2008) 901–906.
[85] S.E. Kabir, A.K. Raha, M.R. Hassan, B.K. Nicholson, E. Rosenberg, A. Sharminc, L. Salassac, Dalton Trans. (2008) 4212–4219.
[86] M.-E. Moret, I. Tavernelli, U. Rothlisberger, J. Phys. Chem. B 113 (2009) 7737–7744.
[87] R.J. Frick, T.S. Hofer, A.B. Pribil, B.R. Randolf, B.M. Rode, J. Phys. Chem. A 113 (2009) 12496–12503.
[88] M.Q. Fatmi, T.S. Hofer, B.R. Randolf, B.M. Rode, J. Comput. Chem. 28 (2007) 1704–1710.
[89] H.K. Khartabil, M.T.C. Martins-Costa, P.C. Gros, Y. Fort, M.F. Ruiz-López, J. Phys. Chem. B 113 (2009) 6459–6467.
[90] T.S. Hofer, B.R. Randolf, B.M. Rode, Chem. Phys. 349 (2008) 210–218.
[91] M.Q. Fatmi, T.S. Hofer, B.R. Randolf, B.M. Rode, J. Phys. Chem. B 112 (2008) 5788–5794.
[92] G. Li, E.M. Sproviero, R.C. Snoeberger III, N. Iguchi, J.D. Blakemore, R.H. Crabtree, G.W. Brudvig, V.S. Batista, Energy Environ. Sci. 2 (2009) 230–238.
[93] D. Duca, F. Ferrante, G.L. Manna, J. Phys. Chem. C 111 (2007) 5402–5408.
[94] V. D'Anna, D. Duca, F. Ferrante, G.L. Manna, Phys. Chem. Chem. Phys. 11 (2009) 4077–4083.
[95] Y. Kameno, A. Ikeda, Y. Nakao, H. Sato, S. Sakaki, J. Phys. Chem. A 109 (2005) 8055–8063.
[96] R. Berthoud, N. Rendón, F. Blanc, X. Solans-Monfort, C. Copéret, O. Eisenstein, Dalton Trans. (2009) 5879–5886.
[97] E. Banach, P. Kozyra, P. Rejmak, E. Brocławik, J. Datka, Catal. Today 137 (2008) 493–497.
[98] T. Archipov, S. Santra, A.B. Ene, H. Stoll, G. Rauhut, E. Roduner, J. Phys. Chem. C 113 (2009) 4107–4116.
[99] B. Kalita, R.C. Deka, J. Phys. Chem. C 113 (2009) 16070–16076.
[100] A.M. Joshi, W.N. Delgass, K.T. Thomson, J. Phys. Chem. C 111 (2007) 11424–11436.
[101] A.M. Joshi, W.N. Delgass, K.T. Thomson, J. Phys. Chem. C 111 (2007) 11888–11896.
[102] W. Panyaburapa, T. Nanok, J. Limtrakul, J. Phys. Chem. C 111 (2007) 3433–3441.
[103] Y. Shiota, K. Suzuki, K. Yoshizawa, Organometallics 25 (2006) 3118–3123.
[104] S. Kasuriya, S. Namuangruk, P. Treesukol, M. Tirtowidjojo, J. Limtrakul, J. Catal. 219 (2003) 320–328.
[105] A. Pianwanit, C. Kritayakornupong, A. Vongachariya, N. Selphusit, T. Ploymeerusmee, T. Remsungnen, D. Nuntasri, S. Fritzsche, S. Hannongbua, Chem. Phys. 349 (2008) 77–82.
[106] C.F. Braga, R.L. Longo, J. Mol. Struct.: THEOCHEM 716 (2005) 33–38.
[107] E. Clot, Eur. J. Inorg. Chem. (2009) 2319–2328.
[108] T.R. Cundari, A. Dinescu, A.B. Kazi, Inorg. Chem. 47 (2008) 10067–10072.
[109] Y. Zhao, D.G. Truhlar, Theor. Chem. Acc. 120 (2008) 215–241.
[110] P.L. Gendre, V. Comte, M.-J. Ondel-Eymin, C. Moïse, E. Pousson, P. Richard, Y. Mugnier, D. Fortin, R.T. Boeré, P.D. Harvey, Inorg. Chem. 48 (2009) 3095–3103.
[111] I.F.D. Hyatt, H.K. Anderson, A.T. Morehead Jr., A.L. Sargent, Organometallics 27 (2008) 135–147.
[112] N. Moldovan, P. Lönnecke, I. Silaghi-Dumitrescu, L. Silaghi-Dumitrescu, E. Hey-Hawkins, Inorg. Chem. 47 (2008) 1524–1531.
[113] H. Suematsu, S. Kanchiku, T. Uchida, T. Katsuki, J. Am. Chem. Soc. 130 (2008) 10327–10337.
[114] D.S. Kuiper, P.T. Wolczanski, E.B. Lobkovsky, T.R. Cundari, J. Am. Chem. Soc. 130 (2008) 12931–12943.
[115] D.S. Kuiper, P.T. Wolczanski, E.B. Lobkovsky, T.R. Cundari, Inorg. Chem. 47 (2008) 10542–10553.
[116] H. Herrmann, J.L. Fillol, H. Wadepohl, L.H. Gade, Organometallics 27 (2008) 172–174.
[117] A. Jimtaisong, L. Feng, S. Sreehari, C.A. Bayse, R.L. Luck, J. Clust. Sci. 19 (2008) 181–195.
[118] Y. Yu, A.R. Sadique, J.M. Smith, T.R. Dugan, R.E. Cowley, W.W. Brennessel, C.J. Flaschenriem, E. Bill, T.R. Cundari, P.L. Holland, J. Am. Chem. Soc. 130 (2008) 6624–6638.
[119] G. Alcaraz, U. Helmstedt, E. Clot, L. Vendier, S. Sabo-Etienne, J. Am. Chem. Soc. 130 (2008) 12878–12879.
[120] B. Dittrich, M.A. Spackman, Acta Cryst. Sect. A A63 (2007) 426–436.
[121] P. Lara, M. Paneque, M.L. Poveda, L.L. Santos, J.E.V. Valpuesta, V. Salazar, E. Carmona, S. Moncho, G. Ujaque, A. Lledós, C. Maya, K. Mereiter, Chem. Eur. J. 15 (2009) 9046–9057.
[122] R.A. Altman, A.M. Hyde, X. Huang, S.L. Buchwald, J. Am. Chem. Soc. 130 (2008) 9613–9620.
[123] E. Zuidema, L. Escorihuela, T. Eichelsheim, J.J. Carbó, C. Bo, P.C.J. Kamer, P.W.N.M. van, Leeuwen, Chem. Eur. J. 14 (2008) 1843–1853.
[124] E. Zuidema, P.W.N.M. van Leeuwen, C. Bo, Organometallics 24 (2005) 3703–3710.
[125] T. Vreven, B. Mennucci, C.O. da Silva, K. Morokuma, J. Tomasi, J. Chem. Phys. 115 (2001) 62–72.
[126] V.P. Ananikov, D.G. Musaev, K. Morokuma, Organometallics 20 (2001) 1652–1667.
[127] V.P. Ananikov, D.G. Musaev, K. Morokuma, J. Am. Chem. Soc. 124 (2002) 2839–2852.
[128] S. Maeda, K. Ohno, J. Phys. Chem. A 109 (2005) 5742–5753.
[129] S. Maeda, K. Ohno, K. Morokuma, J. Chem. Theory Comput. 5 (2009) 2734–2743.
[130] P.J. Donoghue, P. Helquist, P.-O. Norrby, O. Wiest, J. Chem. Theory Comput. 4 (2008) 1313–1323.
[131] P.-O. Norrby, J. Mol. Struct.: THEOCHEM 506 (2000) 9–16.
[132] P.-D. Fan, M. Valiev, K. Kowalski, Chem. Phys. Lett. 458 (2008) 205–209.
[133] G. Brancato, N. Rega, V. Barone, Chem. Phys. Lett. 451 (2008) 53–57.
[134] G. Zheng, H.A. Witek, P. Bobadova-Parvanova, S. Irle, D.G. Musaev, R. Prabhakar, K. Morokuma, J. Chem. Theory Comput. 3 (2007) 1349–1367.
[135] T.D. Iordanov, J. Mol. Struct.: THEOCHEM 850 (2008) 152–159.
[136] M. Lundberg, Y. Sasakura, G. Zheng, K. Morokuma, J. Chem. Theor. Comput., 2010, ASAP. doi:10.1021/ct100029p (available on the web site).
[137] C.H. Suresh, N. Koga, Inorg. Chem. 41 (2002) 1573–1578.
[138] W.P. Giering, A. Prock, A.L. Fernandez, Inorg. Chem. 42 (2003) 8033–8037.
[139] O. Kühl, Coord. Chem. Rev. 249 (2005) 693–704.
[140] C.H. Suresh, Inorg. Chem. 45 (2006) 4982–4986.
[141] J. Mathew, T. Thomas, C.H. Suresh, Inorg. Chem. 46 (2007) 10800–10809.
[142] S. Komin, D. Sebastiani, J. Chem. Theory Comput. 5 (2009) 1490–1498.
[143] V. Vailikhit, W. Treesuwan, S. Hannongbua, J. Mol. Struct.: THEOCHEM 806 (2007) 99–104.
[144] J.L. Lewin, C.J. Cramer, J. Phys. Chem. A 112 (2008) 12754–12760.
[145] H.P. Hratchian, P.V. Parandekar, K. Raghavacharia, M.J. Frisch, T. Vreven, J. Chem. Phys. 128 (2008) 034107.
[146] P.V. Parandekar, H.P. Hratchian, K. Raghavachari, J. Chem. Phys. 129 (2008) 145101.
[147] M.-J. Li, L. Liu, Y. Fu, Q.-X. Guo, J. Mol. Struct.: THEOCHEM 815 (2007) 1–9.
[148] P. Altoè, M. Stenta, A. Bottoni, M. Garavelli, Theor. Chem. Acc. 118 (2007) 219–240.
[149] X. Zeng, H. Hu, X. Hu, W. Yanga, J. Chem. Phys. 130 (2009) 164111.
[150] H. Takahashi, H. Ohno, R. Kishi, M. Nakano, N. Matubayasi, Chem. Phys. Lett. 456 (2008) 176–180.
[151] C.J. Woods, F.R. Manby, A.J. Mulholland, J. Chem. Phys. 128 (2008) 014109.
[152] O. Akin-Ojo, Y. Song, F. Wang, J. Chem. Phys. 129 (2008) 064108.
[153] H.L. Woodcock, W. Zheng, A. Ghysels, Y. Shao, J. Kong, B.R. Brooks, J. Chem. Phys. 129 (2008) 214109.
[154] T. Yamamoto, J. Chem. Phys. 129 (2008) 244104.
[155] M. Lundberg, T. Kawatsu, T. Vreven, M.J. Frisch, K. Morokuma, J. Chem. Theory Comput. 15 (2009) 222–234.
[156] M. Higashi, D.G. Truhlar, J. Chem. Theory Comput. 4 (2008) 790–803.